

High Frequency Dynamics of Amorphous Silica

Jürgen Horbach, Walter Kob*, and Kurt Binder

*Institut für Physik, Johannes Gutenberg-Universität, Staudinger Weg 7, D-55099 Mainz,
Germany*

Abstract

We present the results of extensive molecular dynamics computer simulations in which the high frequency dynamics of silica, $\nu > 0.5$ THz, is investigated in the viscous liquid state as well as in the glass state. We characterize the properties of high frequency sound modes by analyzing $J_l(q, \nu)$ and $J_t(q, \nu)$, the longitudinal and transverse current correlation function, respectively. For wave-vectors $q > 0.4 \text{ \AA}^{-1}$ the spectra are sitting on top of a flat background which is due to multiphonon excitations. In the acoustic frequency band, i.e. for $\nu < 20$ THz, the intensity of $J_l(q, \nu)$ and $J_t(q, \nu)$ in the liquid and the glass approximately proportional to temperature, in agreement with the harmonic approximation. In contrast to this, strong deviations from a linear scaling are found for $\nu > 20$ THz. The dynamic structure factor $S(q, \nu)$ exhibits for $q > 0.23 \text{ \AA}^{-1}$ a boson peak which is located nearly independent of q around 1.7 THz. We show that the low frequency part of the boson peak is mainly due to the elastic scattering of transverse acoustic modes with frequencies around 1 THz. The strength of this scattering depends on q and is largest around $q = 1.7 \text{ \AA}^{-1}$, the location of the first sharp diffraction peak in the static structure factor. By studying $S(q, \nu)$ for different system sizes we show that strong finite size effects are present in the low frequency part of the boson peak in that for small systems part of its intensity is missing. We discuss the consequences of these finite size effects for the structural relaxation.

PACS numbers: 61.20.Lc, 61.20.Ja, 02.70.Ns, 64.70.Pf

Typeset using REVTeX

*Author to whom correspondence should be addressed to: e-mail Walter.Kob@uni-mainz.de

I. INTRODUCTION

The investigation of the vibrational dynamics of supercooled liquids and glasses is a challenging task since these systems do not have the property of translational invariance as it is the case for crystals. Of special interest is the region of intermediate wave-vectors at which collective excitations, i.e. longitudinal and transverse sound waves, begin to experience strongly the structural disorder. Molecular dynamics (MD) simulations are well suited to study vibrational features at these intermediate wave-vectors, say with magnitude $q \geq 0.1 \text{ \AA}^{-1}$, corresponding to frequencies ν in the THz band. This paper is concerned with the simulation of the vibrational dynamics of amorphous silica, which is the prototype of a so-called strong glassformer [1]. Its structure exhibits a medium-range order in that it forms a disordered network of SiO_4 -tetrahedra leading to a peak in the static structure factor around $q = 1.6 \text{ \AA}^{-1}$ [2]. In recent years the high frequency dynamics of silica has been the subject of an intense debate because its Raman and neutron scattering spectra [3,4] show a so-called boson peak around 1 THz, which is also present in many other glassformers but normally gives a less intense contribution to the spectra than in silica. This feature appears also in experiments as an excess over the Debye density of states or, equivalently, over Debye's T^3 -law in the specific heat around the temperature $T = 10 \text{ K}$ [5,6].

Recently it has been shown by means of an inelastic X-ray scattering experiment by Benassi *et al.* [7] that in silica propagating longitudinal sound modes persist up to 0.35 \AA^{-1} , which corresponds to frequencies well above the location of the boson peak. Therefore Benassi *et al.* argued that the boson peak has its origin in these propagating sound modes. In contrast to this suggestion, Vacher *et al.* [8–10] found evidence from the available spectroscopic data that the boson peak is due to the strong scattering of acoustic modes by the disorder thus regarding the boson peak as a manifestation of these strongly scattered modes.

Simple models have been suggested to explain the origin of the boson peak. From the soft potential model [11,12] the idea is put forward that anharmonic localized vibrations coexist with propagating high frequency sound modes in the frequency range around the location of the boson peak. In the case of silica these anharmonic soft modes have been related to coupled SiO_4 -tetrahedra librations [6]. Wischnewski *et al.* [13] have analyzed their neutron scattering data of silica within the soft potential model, and have concluded that the sound waves are indeed scattered from such local vibrational modes below 1 THz, whereas above this frequency static Rayleigh scattering from the atomic disorder takes place. Schirmacher *et al.* [14] have studied a system of coupled harmonic oscillators with a random distribution of force constants. In this model they have found an excess over the Debye behavior in the density of states which they have interpreted as an analogon to the boson peak feature in real structural glasses. In agreement with this model, Sokolov [15] proposed that the boson peak is related to the strong scattering of acoustic like vibrations by fluctuations of the elastic constants.

A feature which shares many properties with the boson peak is also found within the mode-coupling theory (MCT) of the glass transition: In the ideal glass state where all particles are trapped in the cages formed by their neighbors, the spectrum of the density-density correlation function is a superposition of harmonic oscillator spectra which is due to the variety of cages in which the particles are trapped [16]. It is remarkable in this context that the whole light scattering spectra of glycerol, including the boson peak, have

been successfully described within a schematic MCT model [17], and very recently Götze and Mayr have shown that deep inside the glass state, i.e. at temperatures well below the MCT temperature T_c , the theory predicts dynamical features which are very reminiscent to the boson peak [18].

In the last three years MD simulations tried to give insight into the vibrational dynamics of silica [19–24], and other network forming glasses like ZnCl_2 [25]. Most of these investigations have analyzed the dynamics within the harmonic approximation, i.e. by determining the eigenvalues and eigenvectors from the diagonalized dynamical matrix. Although the full information of the vibrational part of the dynamics is given by the eigenmodes (of course only within the harmonic approximation) the origin of the boson peak remains a puzzle. One reason for this is the smallness of the system sizes (20–40 Å) which have been used in the forementioned studies, which has the effect that parts of the boson peak are missing (see below). A second reason is the difficulty of analyzing the boson peak feature in terms of eigenmodes since, as we will discuss in detail below, in the case of silica the coupling of modes with different q is essential for this feature.

In order to avoid these problems we use in the present work a large system size and calculate the exact current and density correlation functions in order to investigate their dependence on wave-vector q and frequency ν . Therefore, we are able to study the temperature dependence of the high frequency dynamics of silica in the liquid state as well as in the glass state. Moreover, we are able to give insight into the relationship between the vibrational dynamics and structural relaxation in the silica melt. The rest of the paper is organized as follows: In the next section we give an overview of the main computational details. In Sec. III we discuss the vibrational dynamics of our silica model by means of the current and density correlation functions. In Sec. IV we summarize and discuss the results.

II. MODEL AND DETAILS OF THE SIMULATIONS

The model potential we use to describe the interactions between the ions in silica is the one proposed by van Beest, Kramer, and van Santen (BKS) [26] which has the following functional form:

$$\phi(r) = \frac{q_\alpha q_\beta e^2}{r} + A_{\alpha\beta} \exp(-B_{\alpha\beta} r) - \frac{C_{\alpha\beta}}{r^6} \quad \alpha, \beta \in [\text{Si}, \text{O}]. \quad (1)$$

Here r is the distance between an ion of type α and an ion of type β . The values of the parameters $A_{\alpha\beta}$, $B_{\alpha\beta}$ and $C_{\alpha\beta}$ can be found in the original publication. The Coulombic part of the potential was evaluated by means of Ewald sums for which further details can be found elsewhere [27]. In recent simulations [27–31] it has been shown that the BKS potential (1) reproduces many static and dynamic properties of real silica very well and thus it can be considered as a reliable model for this material.

We have simulated a system with 8016 ions. The size of the simulation box was fixed to 48.365 Å corresponding to a density of 2.37 g/cm³. Thus, the smallest wave-vector of our simulation has magnitude $q = 0.13 \text{ \AA}^{-1}$. In order to study finite size effects we have done also simulations for smaller systems, and the details of these simulations are given below. In the following we will investigate the fully equilibrated liquid state at $T = 6100 \text{ K}$, 3760 K , and 2750 K and the glass state at $T = 1670 \text{ K}$, 1050 K , and 300 K . In the liquid state we

equilibrated the system first at each temperature in the NVT ensemble at each temperature, and after that we started microcanonical simulations by means of the velocity form of the Verlet algorithm. During the equilibration the temperature was kept constant by using a stochastic collision algorithm. The time step we used was 1.6 fs, and in order to improve the statistics we simulated at each temperature two independent runs. At $T = 2750$ K the length of the equilibration runs was 13 million time steps followed by the microcanonical production runs over 12 million time steps, which corresponds to a real time of 20 ns. During the two production runs we have stored on a linear time scale 30 configurations each which have subsequently been used as the starting configuration of a new simulation for investigating the high frequency dynamics. We mention that the pressure at $T = 2750$ K is around 0.9 GPa. Further details on the simulation of the liquid state can be found elsewhere [27]. The starting-point for producing the glass state were two equilibrated configurations at $T = 2900$ K at which the equilibration time was 4 million time steps (6.5 ns real time). By coupling the system to an external heat bath the temperature was then decreased linearly in time within one million time steps to 0 K. This corresponds to a cooling rate of about $1.8 \cdot 10^{12}$ K/s. During the cooling procedure we stored configurations at the temperatures mentioned above which we used as starting configurations in order to anneal the system for $5 \cdot 10^5$ time steps at constant temperature. Afterwards we propagated the system over $5 \cdot 10^5$ time steps in the microcanonical ensemble and stored configurations every 10^5 time steps. Thus at the end we had at each of the three temperatures in the glass state 22 starting configurations for the investigation of the high frequency dynamics. The pressure for our glass structures is 0.52 GPa at $T = 300$ K, 0.69 GPa at $T = 1050$ K, and 0.8 GPa at $T = 1670$ K.

In this paper we are mainly interested in frequency dependent correlation functions. Therefore time Fourier transformations have to be calculated which we have done by means of the Wiener–Khinchin theorem. It says that the Fourier transformation of a correlation function $C(t) = \langle x(t)x(0) \rangle$ ($x(t)$: density, longitudinal current, transverse current) is given by the power spectrum $Z(\nu) = |a(\nu)|^2$ where $a(\nu)$ denotes the Fourier transform of the time series $x(t)$. The time series were transformed via fast Fourier transformation whereby we applied a Welch window function [32]. Usually we have calculated the time series for the density and the currents over 8192 time steps (13.4 ps real time) by using the aforementioned starting configurations. This results in a frequency resolution of about 0.1 THz. The reliability of the Fourier transformation was tested by calculating also time series over 16384 time steps and in these test cases we have found indeed identical spectra, at least for $\nu > 0.3$ THz.

III. RESULTS

A. Current correlations

In this section we analyze the vibrational features of our silica model by means of the longitudinal and transverse current correlation function $J_l(q, \nu)$ and $J_t(q, \nu)$, respectively, which depend on the magnitude of the wave-vector \mathbf{q} and the frequency ν . These are defined as [33]

$$J_\alpha(q, \nu) = \frac{1}{N} \int_{-\infty}^{\infty} dt \exp(i2\pi\nu t) \langle \mathbf{j}_\alpha(\mathbf{q}, t) \cdot \mathbf{j}_\alpha(-\mathbf{q}, 0) \rangle \quad (2)$$

where the longitudinal part ($\alpha = l$) and the transverse part ($\alpha = t$) of the total current

$$\mathbf{j}(\mathbf{q}, t) = \sum_k \dot{\mathbf{r}}_k(t) \exp(i\mathbf{q} \cdot \mathbf{r}_k(t)) \quad (3)$$

are given by

$$\mathbf{j}_l(\mathbf{q}, t) = \frac{\mathbf{q}\mathbf{q} \cdot \mathbf{j}(\mathbf{q}, t)}{q^2}, \quad (4)$$

$$\mathbf{j}_t(\mathbf{q}, t) = \mathbf{j}(\mathbf{q}, t) - \frac{\mathbf{q}\mathbf{q} \cdot \mathbf{j}(\mathbf{q}, t)}{q^2}. \quad (5)$$

Fig. 1 shows $J_l(q, \nu)$ and $J_t(q, \nu)$ for different values of q up to 1.0 \AA^{-1} at the temperature $T = 2750 \text{ K}$. We have plotted only the functions for the oxygen–oxygen correlations because the silicon–silicon and the silicon–oxygen correlations exhibit qualitatively the same behavior, which is reasonable for such small wave–vectors. Note that even at the relatively high temperature $T = 2750 \text{ K}$, our SiO_2 model is quite viscous having a viscosity of about 380 P , and moreover, that this temperature is well below the critical temperature of mode–coupling theory, which is at 3330 K [27]. Thus within the framework of MCT we are indeed probing the system deep in the glass regime. In Fig. 1a we show $J_l(q, \nu)$ and $J_t(q, \nu)$ in the frequency range between 0.4 and 1.6 THz for the four lowest q values of our simulation, $q = 0.13 \text{ \AA}^{-1}$, 0.18 \AA^{-1} , 0.23 \AA^{-1} , and 0.26 \AA^{-1} . At $q = 0.13 \text{ \AA}^{-1}$ we recognize that there are two peaks, corresponding to the longitudinal and the transverse part of the current, which are well separated from each other. For increasing wave–vectors these peaks move to higher frequencies whereby their width becomes so large that they overlap more and more with each other. In the following we call the excitations corresponding to these peaks high frequency longitudinal acoustic (LA) modes and high frequency transverse acoustic (TA) modes, respectively. From the figure we see that the TA excitations give the most important contribution to the current spectra in that their amplitude is about a factor 6–8 higher than that of the LA excitations. In the wave–vector range in which the LA and TA modes hybridize one would expect that plane waves are no longer eigenmodes, and in the simulation of Taraskin and Elliott it has indeed been shown explicitly that a longitudinal or transverse plane wave with a q value around 0.2 \AA^{-1} decays into a final state which can be characterized as a superposition of plane waves with different wave–vectors and polarizations, but with the same frequency [20].

At $q = 1.0 \text{ \AA}^{-1}$ (Fig. 1b) the current correlation functions are qualitatively different from those discussed so far at lower q : In the transverse part one observes a plateau between 3 and 11 THz , and in the longitudinal part the LA peak around 16 THz seems to be sitting on top of a flat background. In order to describe in more detail the change in the shape of the spectra that occurs at intermediate values of q , we show in Fig. 2 $J_l(q, \nu)$ and $J_t(q, \nu)$ for the O–O, Si–O, and Si–Si correlations for q up to 1.7 \AA^{-1} . At $q = 0.47 \text{ \AA}^{-1}$ we observe in $J_l(q, \nu)$ for the O–O correlations, apart from the LA peak around 6 THz , a peak around $\nu = 26 \text{ THz}$ corresponding to an optical excitation. Moreover, the intensity of the whole spectrum seems to be enhanced in that the LA and the optical peak sit on top of a flat

background. If q is increased to 1.4 \AA^{-1} the LA peak moves to larger frequencies whereby a shoulder around $\nu = 2 \text{ THz}$ gets more and more pronounced. Also at $q = 1.7 \text{ \AA}^{-1}$ there is a LA peak but now its position has moved back to $\nu = 17 \text{ THz}$, i.e. a smaller frequency than at $q = 1.4 \text{ \AA}^{-1}$. In the case of the Si–O correlations (Fig. 2b) the essential difference to the O–O correlations is the negative amplitude of the LA peak for $q \geq 1.4 \text{ \AA}^{-1}$ which indicates an antiphase motion of the silicon and oxygen atoms. The curves for the Si–Si correlations (Fig. 2c) show essentially only one difference compared to those for the O–O correlations in that the optical band has a higher weight in the spectrum than the LA excitations. This is due to the fact that the silicon atoms are bonded stronger in the tetrahedral network than the oxygen atoms, and thus on small length scales more localized motions have a higher weight in the case of the silicon atoms which corresponds to frequencies in the optical band.

Also in the transverse case for the O–O correlations (Fig. 2d) the whole spectrum sits on top of a flat background. The intensity of the TA peak around 3 THz decreases with increasing q whereas there is an increase in the intensity around 9 THz . As a result a broad flat band is obtained for $\nu < 17 \text{ THz}$. In contrast to the O–O correlations, $J_t(q, \nu)$ for the Si–O correlations (Fig. 2e) shows a strong overall decrease of the intensity if q is increased from 1.0 \AA^{-1} to 1.7 \AA^{-1} . This can be easily understood because at $q = 1.7 \text{ \AA}^{-1}$ the current correlation functions measure to a great extent the single particle motion, and therefore the relative motion of the silicon and oxygen atoms gives only a small contribution to the spectra. The most remarkable feature in $J_t(q, \nu)$ for the Si–Si correlations is again that, compared to the O–O correlations, the optical excitation around 20 THz has a larger amplitude than those of the acoustic band for $q \geq 1.0 \text{ \AA}^{-1}$. The essential result which is shown in the Fig. 2 is that for intermediate values of q the whole spectrum is placed on top of a flat background. A similar feature has also been found by Mazzacurati *et al.* [34] in a Lennard–Jones system. These authors have identified the flat background directly in the spectra and in the participation ratio which measures the number of particles that contribute to the eigenmodes at a certain frequency. At the low frequency edge of the density of states the participation ratio has values expected for localized modes. Such a behavior of the participation ratio has also been found in the case of silica [35]. Mazzacurati *et al.* have explained this behavior by showing that the eigenvectors for low frequencies can be represented by a few long–wavelength standing waves plus a random contribution where the random contribution is seen in the spectrum as the flat background. In a phonon picture one can interpret the flat background as the contribution of multiphonon excitations.

By reading off the peak maxima [36] in $J_l(q, \nu)$ and $J_t(q, \nu)$ corresponding to the longitudinal and transverse acoustic modes one gets dispersion like branches $\nu_l(q)$ and $\nu_t(q)$ which are shown in Fig. 3a for $T = 2750 \text{ K}$ and in Fig. 3b for $T = 300 \text{ K}$. It is remarkable that $\nu_l(q)$ and $\nu_t(q)$ exhibit essentially the same behavior in the viscous liquid state ($T = 2750 \text{ K}$) and the glass state ($T = 300 \text{ K}$). This shows that in this (high) frequency window there is no relevant difference between a viscous liquid and a glass which gives support to the idea of Ref. [18] that in this frequency range the viscous liquid can be treated like a glass. Furthermore, we note that both functions look very similar as in simple liquids [33]: The longitudinal branch $\nu_l(q)$ has a periodic structure with a minimum located around $q_m = 2.8 \text{ \AA}^{-1}$, which is the location of the second sharp diffraction peak in the static structure factor and which corresponds to length scales of intratetrahedral distances [27]. Thus, $q_m/2$ can be interpreted, in analogy to crystals, as a quasi Brillouin zone. The minimum in

$\nu_l(q)$ at q_m can be easily understood since the particles tend to favor relative separations of $2\pi/q_m$, and therefore, at these wavelengths it costs a relatively small amount of energy to excite a collective mode corresponding to a relatively small frequency. That the minimum in $\nu_l(q)$ is not observed at $q = 1.7 \text{ \AA}^{-1}$, the location of the *first* sharp diffraction peak in the static structure factor [27], is due to the fact that this q value corresponds to length scales of connected SiO_4 -tetrahedra, a structural unit which is less stiff than one tetrahedron itself. The behavior of $\nu_l(q)$ is in agreement with the findings in a neutron scattering experiment by Arai *et al.* [37], and was also found in the computer simulations of Taraskin and Elliott [35]. The transverse branch $\nu_t(q)$ becomes rather flat for $q > 0.9 \text{ \AA}^{-1}$ which is an indication of the overdamped character of the TA excitations at these wave-vectors.

Also included in Figs. 3a and 3b are fits of the form $\nu_\alpha(q) = c_\alpha q / (2\pi)$, where c_l and c_t denote the longitudinal and the transverse high frequency sound velocity, respectively. The values for c_α obtained from these fits are given in the figures. We recognize that for q up to around 0.4 \AA^{-1} this linear dispersion law holds, which is expected for propagating sound waves at sufficiently small q . We have determined the longitudinal and transverse sound velocity for all temperatures considered by calculating $c_\alpha = 2\pi\nu_\alpha/q$ for the two lowest q values of our simulation $q = 0.13 \text{ \AA}^{-1}$ and $q = 0.18 \text{ \AA}^{-1}$. The sound velocities obtained in this way are shown in Fig. 4 as a function of temperature. Note that c_α as determined from $q = 0.13 \text{ \AA}^{-1}$ and from $q = 0.18 \text{ \AA}^{-1}$ differ by less than 7 % from each other, which shows that these wave-vectors are small enough to determine c_α reliably. From 3760 K to 6100 K the longitudinal sound velocity decreases by about 50 %. No data is shown for c_t at 6100 K in the figure because at this temperature only a peak at $\nu = 0$ is observed. This behavior is in agreement with hydrodynamics which predicts that transverse fluctuations are transported diffusively and therefore contribute to the spectrum only with a peak at $\nu = 0$. We have found, however, that even at $T = 6100\text{K}$ the restoring forces between the particles are large enough to allow the propagation of TA modes for $q \geq 0.35 \text{ \AA}^{-1}$, which can be inferred by the observation of a crossover from a peak around $\nu = 0$ to a peak at finite frequencies in this region of q . Also included in the figure are the experimental sound velocities measured by Vo-Tanh *et al.* [38] which are multiplied with the factor $\sqrt{2.2/2.37}$. This factor takes into account that the density of our simulation, 2.37 g/cm^3 , is slightly different from the experimental one, which is 2.2 g/cm^3 . With this ‘‘correction’’ the simulation reproduces the experimental data very well, both for the longitudinal and the transverse sound velocities. Note that the experimental data have been obtained by Vo-Tanh *et al.* by means of light scattering experiments for values of q of the order 10^{-3} \AA^{-1} , i.e. about two orders of magnitude below the q values of our study. Since, however, it has been shown by Benassi *et al.* [7] that at least the longitudinal sound velocities do not change in this q range, i.e. essentially the same value for c_l is measured in Brillouin scattering experiments and in X-ray scattering up to $q \approx 0.35 \text{ \AA}^{-1}$, it is reasonable to compare the values of c_α from Ref. [38] with our data.

In order to determine, independent from a model, the width of the peaks corresponding to the LA and TA excitations we have plotted the ratio $J_\alpha(q, \nu) / J_{\alpha, \max}(q, \nu)$ versus $\nu - \nu_\alpha(q)$ where $J_{\alpha, \max}$ denotes the amplitude of $J_\alpha(q, \nu)$ at the maximum frequency $\nu_\alpha(q)$. The resulting curves are shown in Fig. 5a in the longitudinal case for q values up to 2.0 \AA^{-1} and in Fig. 5b in the transverse case for q values up to 0.5 \AA^{-1} from which we have read off the full width at half maximum $\Gamma_\alpha(q)$. We recognize from Fig. 5a that the broadening in the curves for the longitudinal part is non-monotonous for $q > 1.0 \text{ \AA}^{-1}$ whereas the curves in

the transverse case broaden monotonously, as can be seen in Fig. 5b.

The linewidths $\Gamma_\alpha(q)$ obtained in this way are shown in Fig. 6 for the LA and TA modes. We recognize from this figure that a quadratic fit describes the longitudinal half width well in the q interval $0.18 \text{ \AA}^{-1} \leq q \leq 0.5 \text{ \AA}^{-1}$. Such a behavior has also been found in the experiment by Benassi *et al.* [7] which was done at $T = 1050 \text{ K}$. The linear dispersion for $\nu_l(q)$ and the quadratic law $\Gamma_l(q) \propto q^2$ support the picture that for $q < 0.4 \text{ \AA}^{-1}$ the system behaves like an isotropic elastic medium with respect to the propagation of the bare LA phonons. For $q \geq 0.6 \text{ \AA}^{-1}$ $\Gamma_l(q)$ becomes rather flat up to $q = 1.1 \text{ \AA}^{-1}$. Then this function decreases significantly and reaches a minimum in the vicinity of the first sharp diffraction peak at $q = 1.6 \text{ \AA}^{-1}$. This is probably due to the fact that the strong spatial correlations on the length scale of two connected SiO_4 tetrahedra decreases the damping of the LA excitation. It is interesting that in the q range $0.6 \text{ \AA}^{-1} < q < 2.0 \text{ \AA}^{-1}$ the width $\Gamma_l(q)$ is significantly smaller than $\nu_l(q)$ (see Fig. 6) which means that the LA excitations cannot be characterized by a Ioffe–Regel crossover. Note that no data points are available between 1.1 and 1.4 \AA^{-1} because the LA peak overlaps with the optical band in this q range and thus they cannot be identified uniquely.

From Fig. 6 we also see that the transverse peak width $\Gamma_t(q)$ can be described by an effective power law with exponent 2.5, $\Gamma_t(q) \propto q^{2.5}$. Thus, the TA phonons seems to be damped stronger than expected from an isotropic elastic medium which would give an exponent 2. In the q region above 0.5 \AA^{-1} the width $\Gamma_t(q)$ becomes larger than the corresponding location of the maximum of the peak $\nu_t(q)$. Therefore, we observe a Ioffe–Regel crossover in the transverse case where the TA excitations lose their propagative character and become strongly overdamped. Note that this is the q region for which $\nu_t(q)$ becomes more or less flat, in contrast to $\nu_l(q)$.

If the current correlation functions would behave as expected from the harmonic approximation they would simply scale with temperature within the classical treatment of our MD simulation. In order to see to what extent a harmonic approximation holds, we have plotted in Fig. 7 $J_l(q, \nu)/T$ and $J_t(q, \nu)/T$ at $q = 0.26 \text{ \AA}^{-1}$ for the O–O, Si–O, and Si–Si correlations. We recognize from these figures that the different peaks corresponding to the LA and TA excitations fall very well onto one master curve in the whole temperature range $3760 \text{ K} \geq T \geq 300 \text{ K}$. Even for $T = 3760 \text{ K}$ only weak deviations from the curve for $T = 300 \text{ K}$ are visible at low frequencies. In contrast to these acoustic excitations the optical band, i.e. the excitations for $\nu > 20 \text{ THz}$, exhibits strong deviations from a harmonic behavior. In the following we denote the different excitations in the optical band as LO1 and LO2 in the longitudinal case and as TO1, TO2, and TO3 in the transverse case. LO1 and LO2 correspond to the frequencies around 25.5 THz and 35.5 THz, respectively, and TO1, TO2, and TO3 correspond to frequencies around 19 THz, 22.3 THz, and 32.2 THz, respectively. (Note that we have been able to identify the different optical branches as a function of q by observing different peaks at approximately the same frequency for different values of q .) It has been shown by computer simulations [19,39] and experiments [40] that the LO2 and TO2 modes correspond to intra–tetrahedral stretching modes, whereas the optical modes with lower frequencies are mainly due to bending and rocking motions of larger structural units. With decreasing temperature the LO2 and TO2 peaks shift respectively from 32 to 36 THz and from 28.5 to 32 THz and their amplitude increases. The mixing of the TO2 and LO2 modes becomes evident in that a shoulder appears at $T = 300 \text{ K}$ in

$J_l(q, \nu)$ around the frequency of the TO2 peak in $J_t(q, \nu)$ and also in $J_t(q, \nu)$ a feature is seen at the frequency of the LO2 mode. From the figure we also recognize that the optical excitations at lower frequencies than LO2 and TO2 have a weaker temperature dependence. This behavior is reasonable since these modes are, in contrast to LO2 and TO2, more extended since they originate from the inter-tetrahedral motion. Nevertheless, also the LO1 peak increases in amplitude with decreasing temperature and shifts to higher frequencies. The TO1 peak evolves into a double peak structure (TO1 and TO3) in lowering the temperature. In Fig. 8 we show the current correlation functions scaled with temperature at the higher wave-vector $q = 1.7 \text{ \AA}^{-1}$. The current correlation functions still scale approximately linear with temperature for $\nu < 20$ THz. For these frequencies the strongest deviations from such a behavior are found in the peak corresponding to the LA excitations around 18 THz. Moreover the mixing of the LO2 excitations with the TO2 excitations is much stronger at $q = 1.7 \text{ \AA}^{-1}$ than at $q = 0.26 \text{ \AA}^{-1}$. Therefore, at q values around 1.7 \AA^{-1} it makes no sense to distinguish these excitations as transverse and longitudinal ones.

Figures 9 show the locations of all the peaks in $J_{l,t}(q)$ that correspond to the optical excitations that can be identified from the current spectra for the Si-Si and the O-O correlations at the temperatures $T = 300$ K and $T = 2750$ K, respectively. Whereas it is possible to distinguish at $T = 300$ K the LO2 from the TO2 peaks for the whole q range $0.13 \text{ \AA}^{-1} \leq q \leq 4.5 \text{ \AA}^{-1}$, this is not possible at $T = 2750$ K for $q > 2.0 \text{ \AA}^{-1}$ because a strong mixing between LO2 and TO2 occurs for these values of q . The same is the case at $T = 300$ K but at this temperature the LO2 and TO2 branches can be distinguished from each other in that they form a double peak structure in the longitudinal and the transverse part. In Fig. 9a the mixing contributions at $T = 300$ K are plotted as the dashed and solid lines for the Si-Si and O-O correlations, respectively: They show the occurrence of a longitudinal mode in the transverse spectrum and, vice versa, the occurrence of a transverse mode in the longitudinal spectrum. In this context the denotation of the modes as longitudinal and transverse ones means that at very low values of q they are expected to be purely longitudinal and transverse, respectively.

For $T = 300$ K the optical branches at lower frequencies, i.e. LO1, TO1, and TO3, can be clearly identified in the Si-Si correlations and the O-O correlations for $q < 0.8 \text{ \AA}^{-1}$. At larger values of q LO1 and TO3 appear as the dominant contribution in the Si-Si correlations, whereas for the O-O correlations the spectra are dominated by the TO3 excitations in J_l and the LO1 excitations in J_t . At $T = 2750$ K the spectra are less pronounced, and we can identify only the TO1 and the LO1 branch apart from the high frequency band above 30 THz. They are visible in the O-O and the Si-Si correlations for $q < 0.8 \text{ \AA}^{-1}$. At higher q only a broad flat band can be observed in the O-O correlations in the frequency range $20 \text{ THz} > \nu > 25 \text{ THz}$ and in the Si-Si correlations an effective maximum appears around $\nu = 20.5$ THz.

B. Density correlations

Studying the density-density-correlation function in the q - ν -domain, i.e. the dynamic structure factor,

$$S(q, \nu) = \frac{1}{N} \int_{-\infty}^{\infty} dt \left\langle \exp(i2\pi\nu t) \sum_{k,l=1}^N \exp(i\mathbf{q} \cdot (\mathbf{r}_k(t) - \mathbf{r}_l(0))) \right\rangle, \quad (6)$$

is of special interest because this quantity can be directly measured in neutron scattering experiments. $S(q, \nu)$ is related to the longitudinal current correlation function $J_l(q, \nu)$ by the simple equation

$$S(q, \nu) = \frac{q^2}{4\pi^2\nu^2} J_l(q, \nu) \quad (7)$$

which holds because of the continuity equation for particle number conservation [33]. Equation (7) means that $S(q, \nu)$ and $J_l(q, \nu)$ contain the same information but features at lower frequencies are strongly enhanced in $S(q, \nu)$ because of the factor $1/\nu^2$. Moreover, $S(q, \nu)$ exhibits a quasielastic line around $\nu = 0$ whereas $J_l(q, \nu)$ approaches zero for $\nu \rightarrow 0$. Therefore, one has to investigate density fluctuations in order to understand the relationship between vibrational and relaxational dynamics, which is one of the goals of the present section, since the latter is seen mainly at small ν .

In Fig. 10a $S(q, \nu)$ is shown for several values of q at $T = 2750$ K. At the three lowest q values of our simulation, $q = 0.13 \text{ \AA}^{-1}$, 0.18 \AA^{-1} and 0.23 \AA^{-1} , one sees essentially one peak which corresponds to the longitudinal acoustic excitations moving to higher frequencies with increasing q . At higher values of q the LA excitation is only visible as a shoulder until it reaches $q = 1.7 \text{ \AA}^{-1}$ at which it can be identified as a broad peak around $\nu = 17$ THz. The reason why this excitation is relatively hard to see is due to the fact that for $q > 0.23 \text{ \AA}^{-1}$ a second peak is present in $S(q, \nu)$ which is located nearly independent of q around $\nu = 1.7$ THz. This peak is the so-called boson peak which is also seen experimentally for silica in Raman and neutron scattering [3,4]. From the figure we also see that to the left of the boson peak two additional peaks are present. The location of these two peaks is at $\nu = 0.75$ THz and $\nu = 1.05$ THz and we have checked that they are not due to bad statistics nor due to artifacts of the Fourier transformation. In order to discuss their origin we have plotted in Fig. 10b $S(q, \nu)$ at $q = 1.7 \text{ \AA}^{-1}$ and $J_t(q, \nu)$ for the five lowest q values of our simulation $q = 0.13 \text{ \AA}^{-1}$, 0.18 \AA^{-1} , 0.23 \AA^{-1} , 0.26 \AA^{-1} , and 0.29 \AA^{-1} . Also included in Fig. 10b is the sum of these transverse current correlation functions $J_{t,\text{sum}}$ (bold dashed line) which we have tried to scale onto $S(q, \nu)$ by dividing it by 1.6 in order to compare the shape of this function with that of $S(q, \nu)$. From the comparison of $J_{t,\text{sum}}$ with the dynamic structure factor we can conclude that the main contribution to the low frequency part of the boson peak comes from the coupling to the TA modes at $q = 0.13 \text{ \AA}^{-1}$, 0.18 \AA^{-1} , and 0.23 \AA^{-1} . The mechanism of how these modes couple to density fluctuations at higher q , e.g. at 1.7 \AA^{-1} in Fig. 10b, is due to elastic scattering since the energy of the scattered TA modes is conserved. We have seen before that the boson peak can only be observed for $q > 0.23 \text{ \AA}^{-1}$, which is exactly the region of q in which the LA and TA peaks in $J(q, \nu)$ begin to overlap (see Fig. 1a). That the transverse part is of special importance is plausible since the intensity of the TA peaks is a factor 6–8 higher than that of the LA peaks in the current correlation functions at fixed q (see Fig. 1). Note that around $\nu = 1.0$ THz the band of acoustic modes is not dense in our simulation because of the finite size of the simulation box. For this reason one would expect that the intensity of the low frequency part of the boson peak is underestimated by our simulation. But as it is demonstrated by Fig. 10b this

property of the finite size system allows us to identify the influence of the low q TA modes on $S(q, \nu)$ at much larger q and small ν .

One might argue that the experimental result, that the boson peak is observed in the Raman spectra of vitreous silica for q values around 10^{-3} \AA^{-1} , is in contradiction to our simulation in which we find this peak in $S(q, \nu)$ only for $q > 0.23 \text{ \AA}^{-1}$. But this is probably due to the fact that in Raman scattering a strong coupling of the light to the incoherent part of the density fluctuations is present. Indeed in our simulation the boson peak is also visible in the self part of the dynamic structure factor $S_s(q, \nu)$ which is obtained from Eq. (6) for $S(q, \nu)$ by taking into account only the terms with $k = l$ in the sum. As can be seen in Fig. 10c even at $q = 0.13 \text{ \AA}^{-1}$, the smallest accessible wave-vector, we observe the boson peak in $S_s(q, \nu)$ and this quantity also exhibits the sharp peaks around $\nu = 0.8 \text{ THz}$ and $\nu = 1.05 \text{ THz}$ that stem from the TA modes. Furthermore, the shape of the different curves in this figure seems to be independent of q . If this is the case this means that $S_s(q, \nu)$ can be factorized into a q dependent part and a purely frequency dependent part. Indeed this has been predicted recently in an analytic calculation by Götze and Mayr [18] for a hard sphere system within the mode coupling theory of the glass transition, and they found that the q dependent part is proportional to q^2 . In order to test whether this prediction holds we have plotted $S_s(q, \nu)/q^2$ for silicon and oxygen in Figs. 11a and 11b, respectively. We recognize that the curves for $0.13 \text{ \AA}^{-1} \leq q \leq 1.0 \text{ \AA}^{-1}$ fall nicely onto one master curve in the whole frequency range $0.5 \text{ THz} \leq \nu \leq 10 \text{ THz}$ whereas at larger q small deviations from the master curve are visible around the location of the boson peak, $\nu = 1.5 \text{ THz}$. To study the q dependence of $S_s(q, \nu)$ in more detail we show in Fig. 12 a double logarithmic plot of this quantity at the frequencies 1.64 THz, 3.02 THz, 10.01 THz, and 30.02 THz. We see that fits with quadratic laws (bold lines in the figures) hold very well at least for $q < 2.0 \text{ \AA}^{-1}$. This means that the whole spectrum scales with q^2 in this q range. Note that a similar behavior was also found in a simulation of ZnCl_2 [41].

From the harmonic approximation one would expect that $S(q, \nu)$ scales with temperature. For this reason we have plotted in Fig. 13 $S(q, \nu)/T$ as a function of frequency at $q = 1.7 \text{ \AA}^{-1}$ for the temperatures $T = 3760 \text{ K}$, 2750 K , 1670 K , 1050 K , and 300 K . We recognize that the curves for the different temperatures fall roughly on top of each other. This means that also in the region of the boson peak our silica model is quite harmonic even at the relatively high temperature $T = 3760 \text{ K}$. Note that even at this temperature the boson peak feature is present in that a shoulder is formed for frequencies above 0.5 THz .

If it is indeed true that TA modes with $q < 0.2 \text{ \AA}^{-1}$ couple to density fluctuations at higher q giving rise to certain features in the boson peak, such as the additional peak at $\nu = 0.8 \text{ THz}$, then these features should be absent if the system size is so small that it does not allow the propagation of TA modes with $q < 0.2 \text{ \AA}^{-1}$. In order to check this prediction we have calculated $S_s(q, \nu)$ at $T = 3760 \text{ K}$ for the system sizes $N = 336$ and $N = 1002$ in addition to $N = 8016$. As the same density as for $N = 8016$ is used, $\rho_m = 2.37 \text{ g/cm}^3$, the sizes of the simulation boxes are $L = 16.80 \text{ \AA}$ and $L = 24.18 \text{ \AA}$ for $N = 336$ and $N = 1002$, respectively. Thus the smallest q values are $q = 0.37 \text{ \AA}^{-1}$ and $q = 0.26 \text{ \AA}^{-1}$. In Fig. 14a we show the obtained $S_s(q, \nu)$ at $q = 0.37 \text{ \AA}^{-1}$, 1.7 \AA^{-1} , and 4.75 \AA^{-1} for the three system sizes. Whereas the curves for the different system sizes coincide for frequencies that are larger than a weakly N dependent frequency $\nu_{\text{cut}}(N)$, for $\nu < \nu_{\text{cut}}(N)$ the magnitude of $S_s(q, \nu)$ decreases with decreasing N . Independent of q we read off $\nu_{\text{cut}} \approx 1.7 \text{ THz}$ for

$N = 336$ and $\nu_{\text{cut}} \approx 1.2$ THz for $N = 1002$. Both frequencies are marked by vertical lines in Fig. 14a. $\nu_{\text{cut}}(N)$ is indeed just slightly below the frequency of the transverse excitation corresponding to the lowest q value determined by the size of the simulation box. These frequencies are at $\nu = 1.85$ THz for $N = 336$ and at $\nu = 1.35$ THz for $N = 1002$. Thus this is evidence that the missing of the TA modes with $q < 0.2 \text{ \AA}^{-1}$ causes the finite size effects in the small systems.

Due to the sum rule $\int d\nu S_s(q, \nu) = 1$, the loss of intensity in the boson peak below $\nu_{\text{cut}}(N)$ has to be “reshuffled” to smaller frequencies leading to a broadening and an increase of the intensity of the quasielastic line around $\nu = 0$. Since the quasielastic line is outside the frequency resolution of our Fourier transformation the consequences in the change of the quasielastic line can be observed better in the Fourier transform of $S_s(q, \nu)$, i.e. the incoherent intermediate scattering function $F_s(q, t)$ which is defined as

$$F_s(q, t) = \frac{N_\alpha}{N} \int_{-\infty}^{\infty} d\nu \exp(2\pi\nu t) S_s(q, \nu) \quad \alpha \in [\text{Si}, \text{O}] . \quad (8)$$

For oxygen this quantity is shown in Fig. 14b at $q = 1.7 \text{ \AA}^{-1}$ for different system sizes. (We mention that we have also included a curve for $N = 3006$ in the figure. The box length in this case is $L = 34.89 \text{ \AA}$ corresponding to the lowest q value $q = 0.18 \text{ \AA}^{-1}$.) We recognize from Fig. 14b that with decreasing system size the height of the plateau, which is the Lamb–Mössbauer factor, increases and the α –relaxation time shifts to longer times. Furthermore, the scattering functions for the small systems show a pronounced oscillation for $t > 0.2$ ps. This can be simply understood from the ν –dependence of $S_s(q, \nu)$: For $N = 8016$ this quantity shows a shoulder around 1.0 THz which corresponds to the monotonous decay of $F_s(q, t)$. In the small systems there is a peak in $S_s(q, \nu)$ around $\nu_{\text{cut}}(N)$ which corresponds to the oscillations in $F_s(q, t)$ with a period $1/\nu_{\text{cut}}(N)$. From the fact that the band of the transverse acoustic modes is not dense for the region of small q (see Fig. 10c) we expect also for $N = 8016$ that the finite size effects are present. But, since in Fig. 14b the differences of the curves for $N = 3006$ and $N = 8016$ are small, we can conclude that the finite size effects play not an important role for $N = 8016$, at least for $T = 3760$ K. In order to investigate the influence of these finite size effects on the α –relaxation we define the α –relaxation time τ_α as the time at which $F_s(q, t)$ has decayed to $1/e$. τ_α increases from $N = 8016$ to $N = 336$ by about 40 %. However, in the α –relaxation regime the shape of $F_s(q, t)$ does not seem to depend on the system size, as can be seen in the inset of Fig. 14b where we have plotted $F_s(q, t)$ versus the scaled time t/τ_α . We see that in the α –relaxation regime the curves for the different system sizes fall onto one master curve. This holds also for $F_s(q, t)$ for the silicon atoms.

Of course, the finite size effects are also important in the total dynamic structure factor. Figure 15a shows $S(q, \nu)$ for the two system sizes $N = 8016$ and $N = 336$ at $T = 2750$ K and the three q values $q = 0.9 \text{ \AA}^{-1}$, 1.7 \AA^{-1} and 4.75 \AA^{-1} . We can again identify a cut–off frequency around 1.7 THz below which there is a loss of intensity in $S(q, \nu)$ for $N = 336$. Note that the sharp peaks at $\nu = 0.75$ THz and $\nu = 1.05$ THz are again not present in the small system. Moreover, we recognize that the relative intensity loss in the small system compared to the large system depends on q . In order to quantify this q dependence we define the ratio

$$R(q, \nu) := \frac{S_{N=8016}(q, \nu)}{S_{N=336}(q, \nu)} - 1 \quad (9)$$

which is zero if the dynamic structure factor coincides for the two system sizes. Figure 15b shows $R(q, \nu)$ for several values of q . Its behavior underlines what we have said before that the low frequency part of the boson peak is mainly due to the elastic scattering of the two TA modes with the frequencies $\nu = 0.75$ THz and $\nu = 1.05$ THz corresponding to the lowest q values of our simulation for the system size $N = 8016$. Obviously, the amplitudes of the peaks in $R(q, \nu)$ do not change monotonously as a function of q . In order to investigate this q dependence $R(q, \nu)$ is plotted in Fig. 15c for the frequencies $\nu = 0.75$ THz and $\nu = 1.05$ THz as a function of q . $R(q, \nu)$ shows pronounced maxima at $q = 1.6 \text{ \AA}^{-1}$, i.e. in the vicinity of the location of the first sharp diffraction peak in the static structure factor, and at $q = 2.8 \text{ \AA}^{-1}$, which is the location of the second peak in $S(q, \nu)$. Thus, the structural disorder on intermediate length scales, i.e. the length scale introduced by two connected SiO_4 -tetrahedra, is most relevant for the scattering of the TA modes with $q < 0.2 \text{ \AA}^{-1}$. Also included is $R_s(q, \nu)$ for the two frequencies which is obtained by putting in $S_s(q, \nu)$ instead of $S(q, \nu)$ into the definition (9). The incoherent part $R_s(q, \nu)$ decreases monotonously with q which is plausible since the finite size effects should vanish at very large values of q corresponding to small length scales.

IV. SUMMARY AND CONCLUSIONS

We have done molecular dynamics simulations in order to investigate the high frequency dynamics of amorphous silica. The results which we have presented in this paper have been for the fully equilibrated liquid and the glass state. The frequency range we have studied is $0.5 \text{ THz} < \nu < 40 \text{ THz}$ for wave-vectors with magnitude $q \geq 0.13 \text{ \AA}^{-1}$ (limited by the size of the simulation box).

In a first step we have discussed the properties of the longitudinal and transverse current correlation functions. At low frequencies we have identified propagating longitudinal acoustic (LA) and transverse acoustic (TA) modes the maxima of which move to higher frequencies with increasing q . The amplitude of the TA peaks is a factor 6–8 larger than that of the LA peaks at a fixed value of q which is a first indication for the importance of the transverse dynamics in silica. Whereas the LA peak is separated quite well from the TA peak on the frequency axis at $q = 0.13 \text{ \AA}^{-1}$, both peaks begin to overlap at higher q . The q region at which the LA and TA peaks begin to overlap significantly can be seen as a crossover region from a regime where the longitudinal and transverse modes exhibit only a weak interaction to a regime where a strong interaction between different modes is present. One important sign of this is that the qualitative shape of the spectra starts to change gradually around $q = 0.6 \text{ \AA}^{-1}$: The LA peaks are still well-defined, but they are now sit on top of a flat background. The acoustic band in $J_t(q, \nu)$ shows a similar behavior in that it evolves into a broad plateau from about 3 to 11 THz. The observation that the acoustic modes are located on top of a flat background for intermediate values of q has recently been found by Götze and Mayr [18] as an essential result in an analytic calculation of the spectra of hard sphere systems in their glass state within the mode-coupling theory of the glass transition. Within their theory Götze and Mayr have explained the existence of the flat background spectrum by the presence of inelastic phonon scattering where a mode decays into two modes due to anharmonicity. In the same sense we can understand the flat background spectrum in silica as the manifestation of multiphonon excitations.

By reading off the peak maxima in $J_l(q, \nu)$ and $J_t(q, \nu)$ as a function of q one obtains dispersion like functions $\nu_l(q)$ and $\nu_t(q)$ for the longitudinal and transverse part, respectively. $\nu_l(q)$ shows an approximately linear behavior for wave-vectors up to 0.3 \AA^{-1} . On the other hand the full width at half maximum $\Gamma_l(q)$ of the LA peaks is well described by a quadratic law for $q \leq 0.5 \text{ \AA}^{-1}$. This means that to a good approximation the system behaves like an isotropic elastic medium up to $q \approx 0.3 \text{ \AA}^{-1}$ with respect to the longitudinal sound modes. Furthermore, $\nu_l(q)$ exhibits a quasi Brillouin zone at $q_m/2$ where q_m is the location of the second sharp diffraction peak in the static structure factor corresponding to length scales of intratetrahedral distances. Also $\nu_t(q)$ shows approximately a linear behavior at small q . But the data for $\Gamma_t(q)$ cannot be described by a quadratic law. Instead, $\Gamma_t(q)$ is fitted well with a $q^{2.5}$ law from which we conclude that the TA excitations are stronger damped than expected from an isotropic elastic medium. For $q > 0.8 \text{ \AA}^{-1}$ $\nu_t(q)$ becomes flat, and in the same range the TA excitations become strongly overdamped in that they reach a Ioffe–Regel limit, i.e. $\Gamma_t(q)$ is of the order of $\nu_t(q)$. We emphasize that there are no peculiarities in the qualitative behavior of $\nu_l(q)$ and $\nu_t(q)$ for our silica model since these functions look very similar for simple liquids [33].

From the two lowest q values of our simulation, $q = 0.13 \text{ \AA}^{-1}$ and 0.18 \AA^{-1} , we have determined the apparent high frequency sound velocities for the different temperatures and find that they reproduce the light scattering data by Vo–Tanh *et al.* [38] very well. Thus this is another example that the BKS model is able to reproduce reliably the experimental data of amorphous silica.

Most of the results we have summarized up to now for the acoustic band are for the silica melt at $T = 2750 \text{ K}$. But we have seen that in the temperature range $300 \text{ K} \leq T \leq 3760 \text{ K}$ the spectra scale to a good approximation linearly with temperature for frequencies $\nu < 20 \text{ THz}$, a behavior which is expected if the harmonic approximation is valid. The linear scaling is not valid for the complex optical bands above 20 THz . For these excitations the spectrum becomes more pronounced with decreasing temperature. If one plots the current correlation functions divided by temperature one recognizes that the peak maxima corresponding to the intratetrahedral stretching modes LO2 and TO2 move to higher frequencies and also their amplitude increases with decreasing temperature. This is just the result of the fact that the particles are more localized the lower the temperature is, which causes anharmonicities to disappear. Nevertheless, due to the disorder, especially for the LO2 and TO2 modes, a strong mixing occurs between the longitudinal and the transverse part for $q > 0.3 \text{ \AA}^{-1}$ which can be clearly identified at $T = 300 \text{ K}$. So, these wave-vectors are no longer good quantum numbers, and if one treats disordered structures within the harmonic approximation one has to keep in mind that this approximation only describes the “mixing contributions” in an effective way.

In a second step we have discussed density fluctuations by means of the dynamic structure factor $S(q, \nu)$. For $q > 0.23 \text{ \AA}^{-1}$ this quantity exhibits a boson peak which is located nearly q independent around $\nu_{\text{BP}} = 1.7 \text{ THz}$ at $T = 2750 \text{ K}$. The boson peak excitations coexist with the LA modes since the latter is visible also at frequencies above ν_{BP} . Since the boson peak has a much larger intensity than the LA peak, e.g. a factor of 7–8 for $q = 1.0 \text{ \AA}^{-1}$, the LA excitations are visible only as a shoulder in $S(q, \nu)$. Only if the LA peak has moved to high frequencies, e.g. to 17 THz at $q = 1.7 \text{ \AA}^{-1}$, one observes this peak as a second peak in addition to the boson peak in the dynamic structure factor. In the low frequency part of the

boson peak two sharp peaks are present at $\nu = 0.75$ THz and $\nu = 1.05$ THz which are due to the elastic scattering of the TA modes with $q = 0.13 \text{ \AA}^{-1}$ and $q = 0.18 \text{ \AA}^{-1}$, respectively. We will discuss them in more detail below. Also the dynamic structure factor $S(q, \nu)$ scales for frequencies around ν_{BP} roughly with temperature in the range $3760 \text{ K} \geq T \geq 300 \text{ K}$. Note that at $T = 3760 \text{ K}$ the boson peak feature can be only seen as a shoulder which grows out of the quasielastic line. The fact that the boson peak can be seen even at such high temperatures supports the view of Ref. [18] that this feature becomes visible as soon as temperature is around T_c , which for our system is around 3330 K [27].

For wave-vectors up to about $1\text{--}2 \text{ \AA}^{-1}$ the self part of the dynamic structure factor $S_s(q, \nu)$ exhibits a factorization into a frequency dependent and wave-vector dependent part whereby the latter is proportional to q^2 . Apart from the fact that this property of $S_s(q, \nu)$ has also been found in a MD simulation of ZnCl_2 [41] it is remarkable that this result comes out of the mode coupling calculation of Goetze and Mayr [18]. So this is another important feature which is reproduced by this theoretical approach.

In order to get more insight into the boson peak feature we have done simulations also for smaller system sizes than the normally used system with $N = 8016$ particles. We have found strong finite size effects in the low frequency part of the boson peak which can be characterized by a frequency $\nu_{\text{cut}}(N)$ below which there is a lack of intensity in the dynamic structure factor. The frequency $\nu_{\text{cut}}(N)$ decreases with increasing system size N and is essentially independent of q . The reason for these finite size effects is due to the absence of the TA excitations with $q < 0.2 \text{ \AA}^{-1}$ in the small systems since the smallest q value of our simulations with $N = 1002$ and $N = 336$ particles are 0.26 \AA^{-1} and 0.37 \AA^{-1} , respectively. In the time domain, i.e. in the incoherent intermediate scattering function $F_s(q, t)$, the finite size effects cause an increase of the Lamb–Mössbauer factor and of the α –relaxation time. This is a consequence of the sum rule $\int d\nu S_s(q, \nu) = 1$ since the missing of intensity for $\nu < \nu_{\text{cut}}(N)$ has to be “reshuffled” to smaller frequencies. Because of the abrupt decrease of $S_s(q, \nu)$ below $\nu_{\text{cut}}(N)$ for small N we observe quite pronounced oscillations for $t > 0.2 \text{ ps}$ in $F_s(q, t)$ whereby the period of these oscillations is approximately equal to $\nu_{\text{cut}}(N)$. Note that a similar behavior was also found in a MD simulation by Lewis and Wahnström [42] for a model of orthoterphenyl in which the interactions between the molecules are described by a Lennard–Jones potential. These authors have suggested that a disturbance that propagates through the system will leave and reenter the box due to the periodic boundary conditions after a time L/c , where L is the size of the box and c is the typical velocity of the sound wave. This mechanism then produces an echo, i.e. an additional signal which produces the slowed down decay of the correlation functions like $F_s(q, t)$. We have also suggested this explanation recently for silica [43], but we think now that this explanation for the finite size effects is not the correct one. Instead, the general argument is that in small enough systems (with a smallest wave-vector with magnitude q_s) parts of the vibrational spectrum are missing below a frequency $\nu_{\text{cut}}(N)$ because of the coupling to wave-vectors with $q < q_s$ occurring in an infinite system. In a Lennard–Jones system such a coupling is reflected in the flat background spectrum which was shown to be present by Mazzacurati *et al.* [34]. In the case of silica there is in addition the coupling which arises from the elastic scattering of transverse TA modes with small q by the structural disorder.

One may speculate that the strength of the boson peak in silica is due the strong coupling of the TA excitations to the longitudinal part. The stiffness of the tetrahedral SiO_2 network

introduces strong restoring forces which allow the propagation of shear waves with a large amplitude even at relatively high temperatures. We have shown that the strongest scattering of the TA modes is at $q \approx 1.6 \text{ \AA}^{-1}$. This is in agreement with suggestions in the literature that the boson peak is caused by the interactions of sound modes with coupled rotations of several tetrahedra [6,35]. A possible mechanism of this interaction would be that the coupled rotations of the tetrahedra enable the change of the polarization of transverse acoustic modes, so that they contribute to the density fluctuation spectrum, i.e. constituting at least part of the boson peak.

Acknowledgments: We thank A. Latz, M. Letz, W. Götze, G. Ruocco, and F. Sciortino for many stimulating discussions during this work. We also thank D. Vo-Tanh for providing us with the light scattering data of the sound velocities. This work was supported by BMBF Project 03 N 8008 C and by SFB 262/D1 of the Deutsche Forschungsgemeinschaft. We also thank the HLRZ Jülich for a generous grant of computer time on the CRAY-T3E.

REFERENCES

- [1] C. A. Angell, in *Relaxation in Complex systems*, edited by K. L. Ngai and G. B. Wright (U.S. Department, Commerce, Springfield, MA, 1985).
- [2] D. L. Price and J. M. Carpenter, *J. Non-Cryst. Solids* **92**, 153 (1987).
- [3] G. Winterling, *Phys. Rev. B* **12**, 2432 (1975).
- [4] M. Foret, E. Courtens, R. Vacher, and J.-B. Suck, *Phys. Rev. Lett.* **77**, 3831 (1996).
- [5] R. C. Zeller and R. O. Pohl, *Phys. Rev. B* **4**, 2029 (1971).
- [6] U. Buchenau, M. Prager, N. Nücker, A. J. Dianoux, N. Ahmad, and W. A. Phillips, *Phys. Rev. B* **34**, 5665 (1986).
- [7] P. Benassi, M. Krisch, C. Masciovecchio, V. Mazzacurati, G. Monaco, G. Ruocco, F. Sette, and R. Verbeni, *Phys. Rev. Lett.* **77**, 3835 (1996).
- [8] R. Vacher, J. Pelous, and E. Courtens, *Phys. Rev. B* **56**, R481 (1997).
- [9] R. Vacher, M. Foret, E. Courtens, J. Pelous, and J. B. Suck, *Phil. Mag. B* **77**, 523 (1998).
- [10] E. Rat, M. Foret, E. Courtens, R. Vacher, and M. Arai, *Phys. Rev. Lett.* **83**, 1355 (1999).
- [11] V. G. Karpov, M. I. Klinger, and F. N. Ignatiev, *Sov. Phys. JETP* **57**, 439 (1983).
- [12] U. Buchenau, Y. M. Galperin, V. L. Gurevich, D. A. Parshin, M. A. Ramos, and H. R. Schober, *Phys. Rev. B* **46**, 2798 (1992).
- [13] A. Wischnewski, U. Buchenau, A. J. Dianoux, W. A. Kamitakahara, and J. L. Zarestky, *Phys. Rev. B* **57**, 2663 (1998).
- [14] W. Schirmacher, G. Diezemann, and G. Ganter, *Phys. Rev. Lett.* **81**, 136 (1998).
- [15] A. P. Sokolov, *J. Phys.: Condens. Matter* **11**, A213 (1999).
- [16] W. Götze, *Z. Phys. B* **56**, 139 (1984).
- [17] T. Franosch, W. Götze, M. R. Mayr, and A. P. Singh, *Phys. Rev. E* **55**, 3183 (1997).
- [18] W. Götze and M. R. Mayr, *Phys. Rev. E*, in press.
- [19] S. N. Taraskin and S. R. Elliott, *Phys. Rev. B* **56**, 8605 (1997).
- [20] S. N. Taraskin and S. R. Elliott, *J. Phys.: Condens. Matter* **11**, A219 (1999).
- [21] S. N. Taraskin and S. R. Elliott, *Phys. Rev. B* **59**, 8572 (1999).
- [22] B. Guillot and Y. Guissani, *Phys. Rev. Lett.* **78**, 2401 (1997).
- [23] J. Horbach, W. Kob, and K. Binder, *J. Non-Cryst. Solids* **235–237**, 320 (1998).
- [24] R. Dell’Anna, G. Ruocco, M. Sampoli, and G. Viliani, *Phys. Rev. Lett.* **80**, 1236 (1998).
- [25] M. C. C. Ribeiro, M. Wilson, and P. A. Madden, *J. Chem. Phys.* **108**, 9027 (1998).
- [26] B. W. H. van Beest, G. J. Kramer, and R. A. van Santen, *Phys. Rev. Lett.* **64**, 1955 (1991).
- [27] J. Horbach and W. Kob, *Phys. Rev. B* **60**, 3169 (1999).
- [28] J. Horbach, W. Kob, and K. Binder, *J. Phys. Chem. B* **103**, 4104 (1999).
- [29] K. Vollmayr, W. Kob, and K. Binder, *Phys. Rev. B* **54**, 15808 (1996).
- [30] T. Koslowski, W. Kob, and K. Vollmayr, *Phys. Rev. B* **56**, 9469 (1997).
- [31] P. Jund and R. Jullien, to appear in *Phys. Rev. B*, preprint cond-mat/9903033.
- [32] W. H. Press, B. P. Flannery, S. A. Teukolsky, and W. T. Vetterling, *Numerical Recipes* (Cambridge University Press, Cambridge, 1986).
- [33] J. P. Boon and S. Yip, *Molecular Hydrodynamics* (Dover Publications, New York, 1980).
- [34] V. Mazzacurati, G. Ruocco, and M. Sampoli, *Europhys. Lett.* **34**, 681 (1996).
- [35] S. N. Taraskin and S. R. Elliott, *Europhys. Lett.* **39**, 37 (1997).

[36] In order to obtain the peak maxima $\nu_\alpha(q)$ we have used the formula

$$J_\alpha(q, \nu) = \frac{A_\alpha(q)\nu^2}{(\nu^2 - \nu_\alpha^2)^2 + (B_\alpha(q)\nu)^2}. \quad (10)$$

which contains the fit parameters $A_\alpha(q)$, $B_\alpha(q)$, and $\nu_\alpha(q)$. Note that Eq. (10) has the same form as the solution of the linearized Navier–Stokes equation for $J_l(q)$, when the heat mode is neglected [33]. We emphasize that we have used Eq. (10) only as a fit formula to determine $\nu_\alpha(q)$. Therefore, we have applied Eq. (10) only in a small interval around the location of the maximum position $\nu_\alpha(q)$.

- [37] M. Arai, Y. Inamura, and A. C. Hannon, *Physica B* **263/264**, 268 (1999).
- [38] D. Vo-Tanh, A. Polian, and P. Richet, preprint (1999).
- [39] A. Pasquarello and R. Car, *Phys. Rev. Lett.* **80**, 5145 (1998).
- [40] F. L. Galeener, *Phys. Rev. B* **19**, 4292 (1979).
- [41] M. Foley, M. Wilson, and P. A. Madden, *J. Chem. Phys.* **108**, 9027 (1998).
- [42] L. J. Lewis and G. Wahnström, *Phys. Rev. E* **50**, 3865 (1994).
- [43] J. Horbach, W. Kob, K. Binder, and C. A. Angell, *Phys. Rev. E* **54**, R5897 (1996).

FIGURES

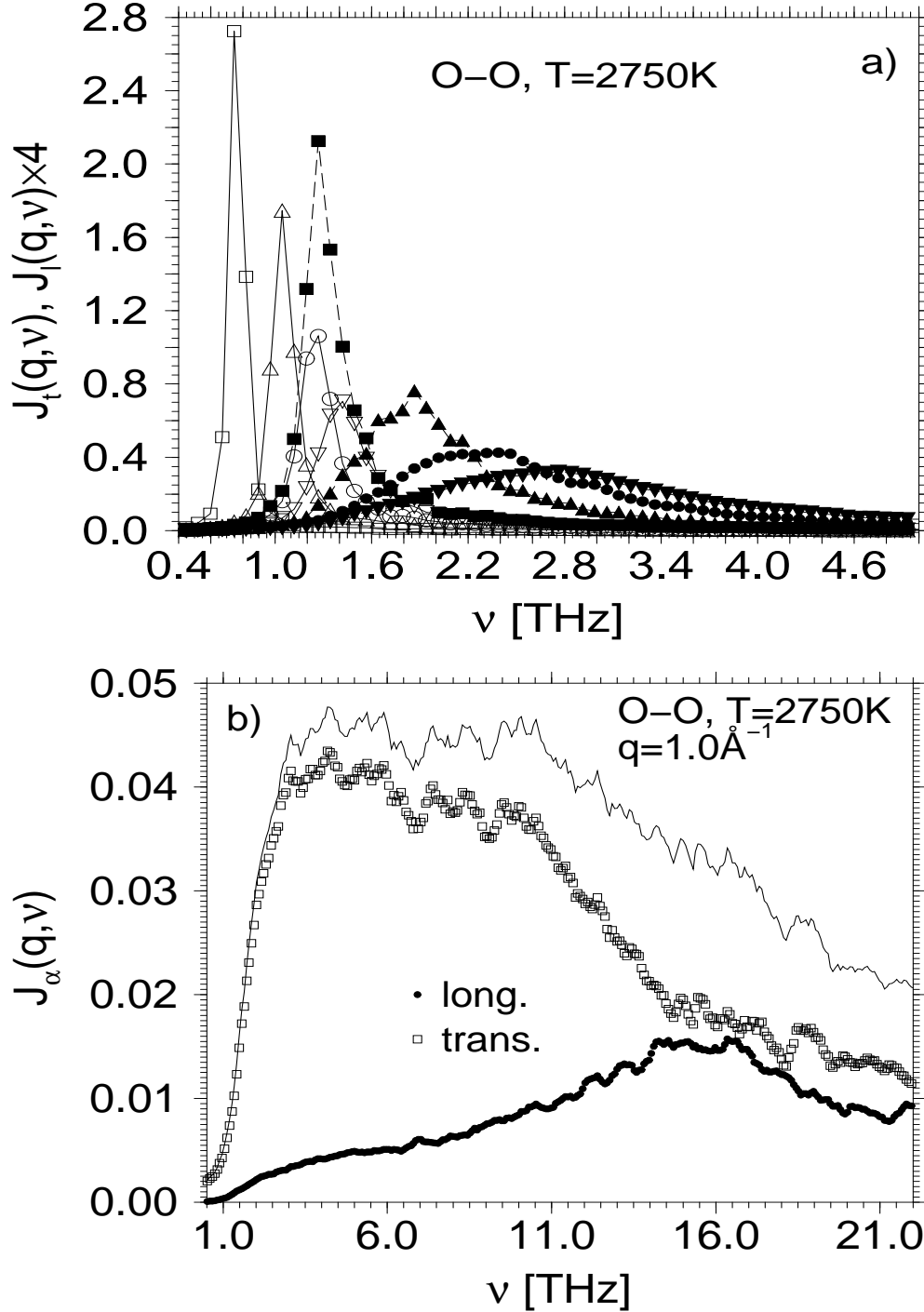


FIG. 1. Longitudinal and transverse current correlation functions (filled and open symbols, respectively) for the oxygen–oxygen correlations at the temperature $T = 2750$ K. a) The peaks moving to higher frequencies correspond to $q = 0.13 \text{ \AA}^{-1}$, $q = 0.18 \text{ \AA}^{-1}$, $q = 0.23 \text{ \AA}^{-1}$, and $q = 0.26 \text{ \AA}^{-1}$ for the longitudinal and transverse functions, respectively. Note that the curves for $J_l(q, \nu)$ are multiplied by a factor of 4. b) $q = 1.0 \text{ \AA}^{-1}$. The solid line corresponds to the sum of J_l and J_t .

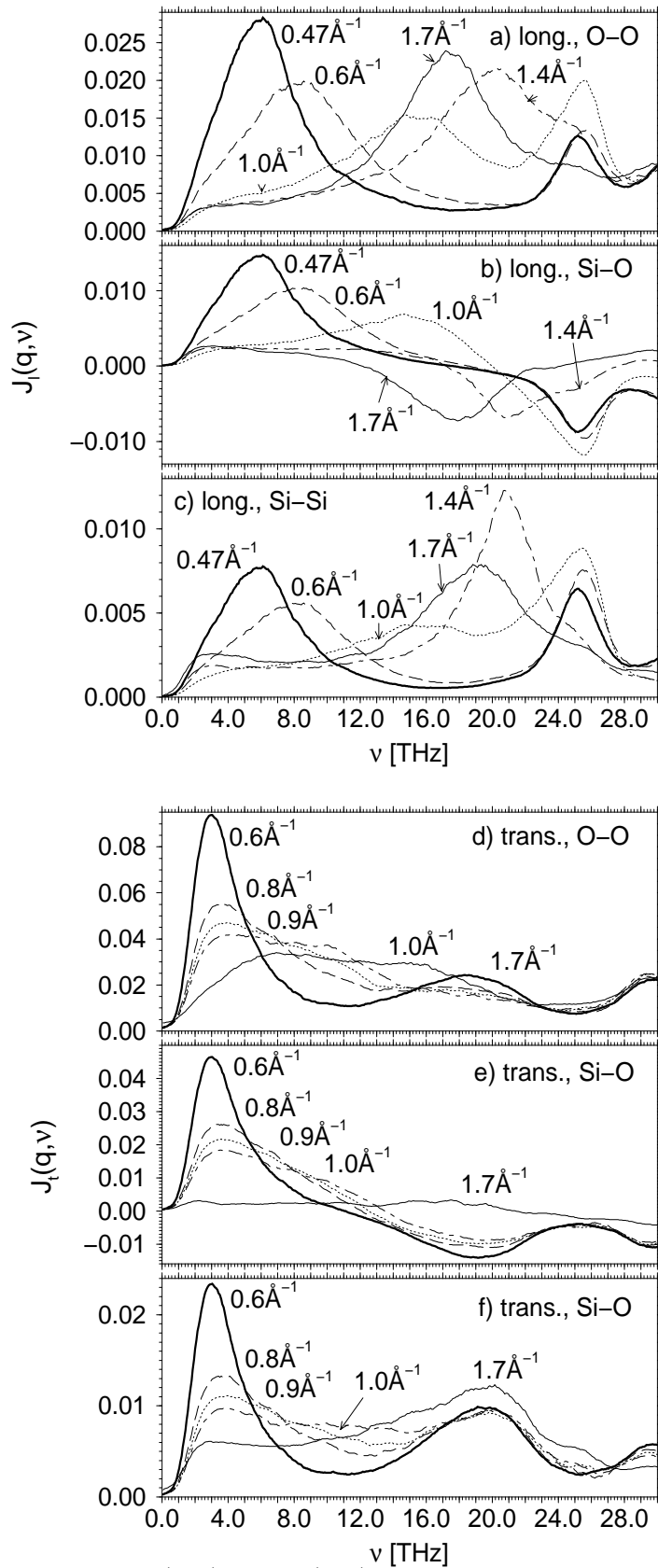


FIG. 2. $J_l(q, \nu)$ and $J_t(q, \nu)$ for various wave-vectors at $T = 2750$ K, a) J_l for O-O, b) J_l for Si-O, c) J_l for Si-Si, d) J_t for O-O, e) J_t for Si-O, f) J_t for Si-Si.

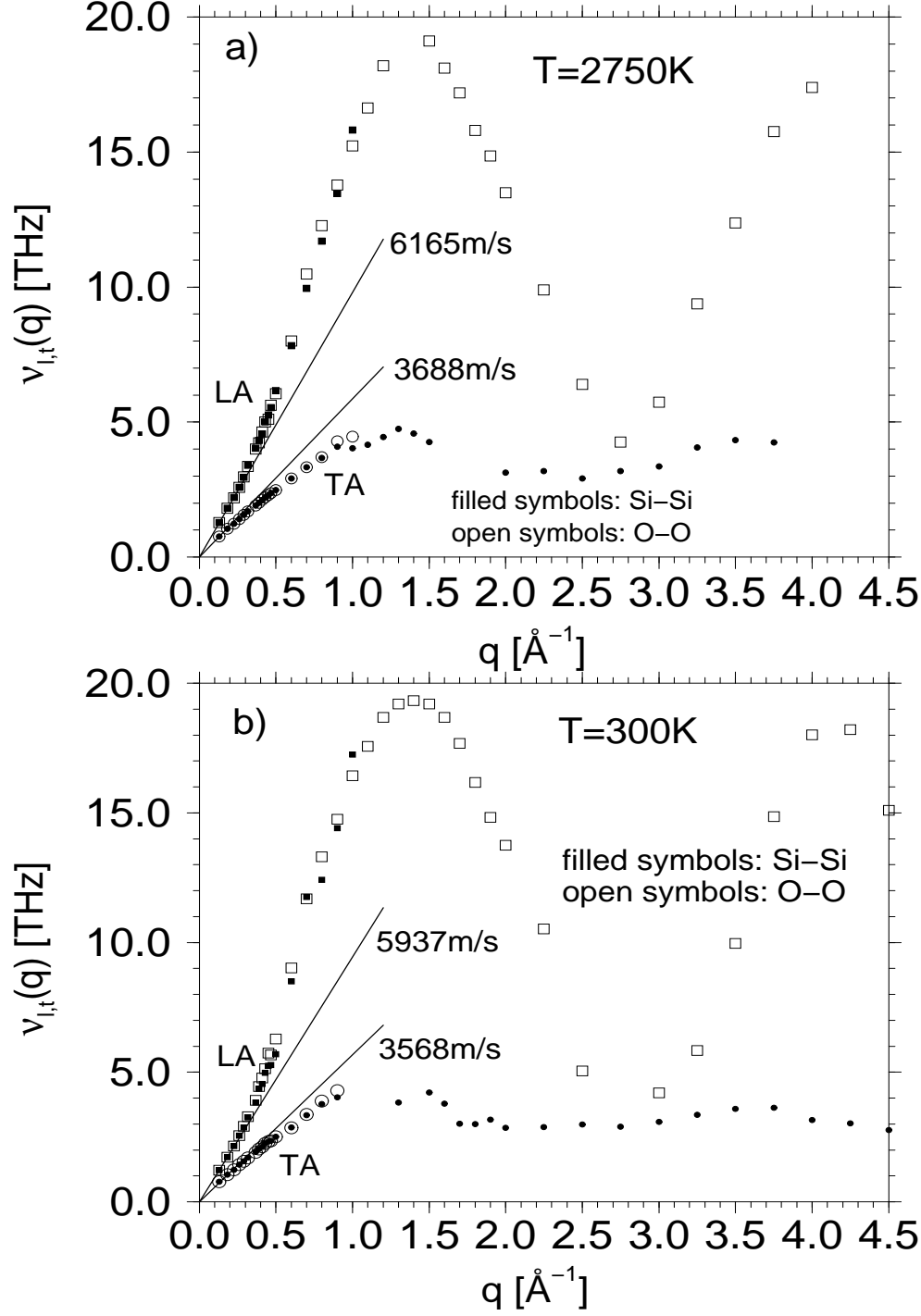


FIG. 3. Peak maximum position $\nu_{l,t}(q)$ for the LA and TA modes for the Si-Si correlations (filled symbols) and the O-O correlations (open symbols) at a) $T = 2750\text{ K}$ and b) $T = 300\text{ K}$. The bold lines are fits with linear laws $\nu_\alpha = c_\alpha q / (2\pi)$ for which the corresponding values for the sound velocities c_α are given in the figure.

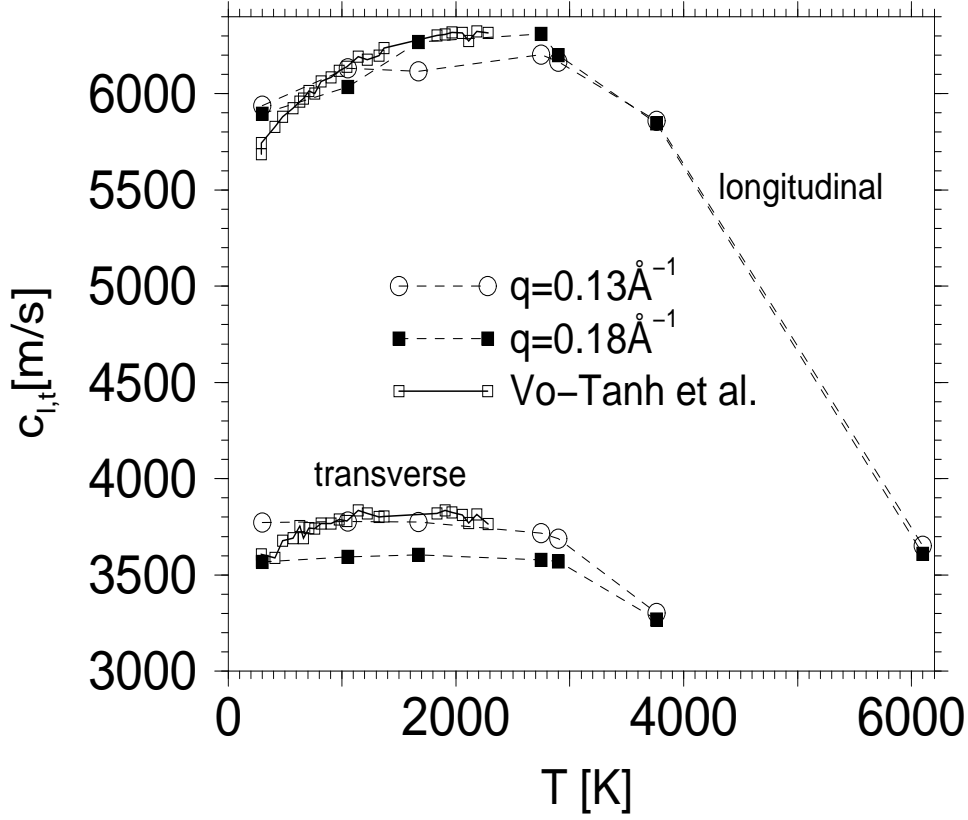


FIG. 4. The temperature dependence of the sound velocities $c_{l,t}$ which are determined from $\nu_{l,t}(q)$ at $q = 0.13 \text{ \AA}^{-1}$ (open circles) and $q = 0.18 \text{ \AA}^{-1}$ (filled squares). Also included are the experimental data of Vo-Tanh *et al.* [38] which we have multiplied with the factor $(2.2/2.37)^{0.5}$ in order to take into account the different density of our simulation from that of the experiment.

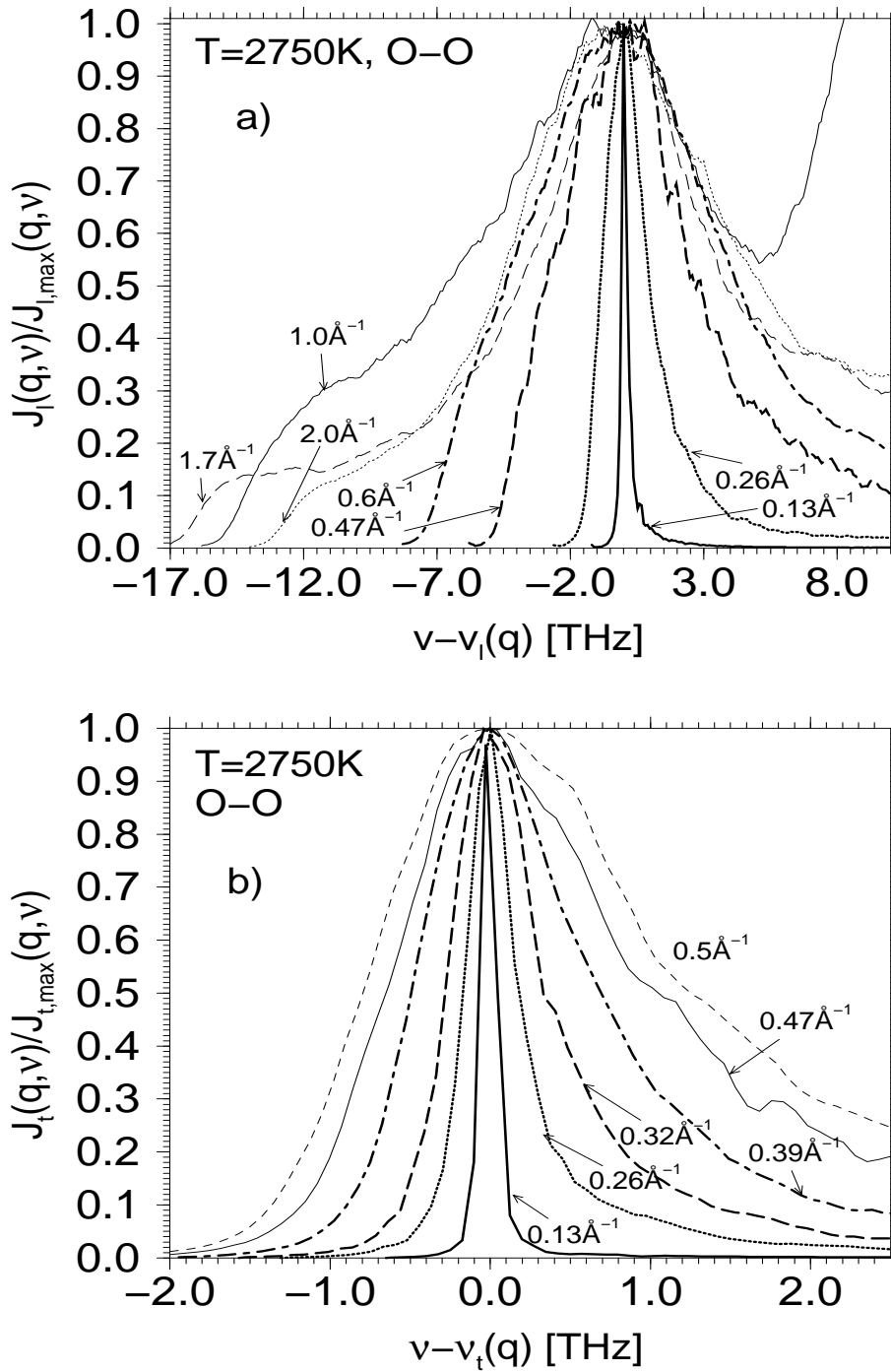


FIG. 5. a) $J_l(q, \nu)/J_{l, \max}$ versus $\nu - \nu_l(q)$ at $T = 2750$ K for the O-O correlations in the q range $0.13 \text{ \AA}^{-1} \leq q \leq 2.0 \text{ \AA}^{-1}$. b) $J_t(q, \nu)/J_{t, \max}$ versus $\nu - \nu_t(q)$ at $T = 2750$ K for the O-O correlations in the q range $0.13 \text{ \AA}^{-1} \leq q \leq 0.5 \text{ \AA}^{-1}$.

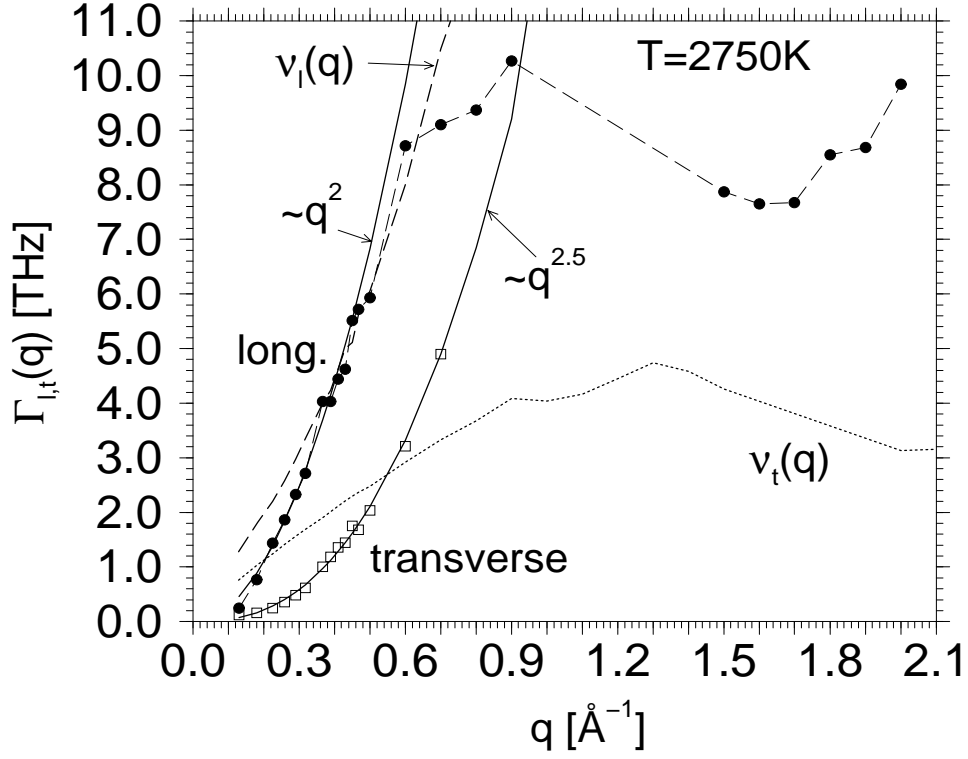
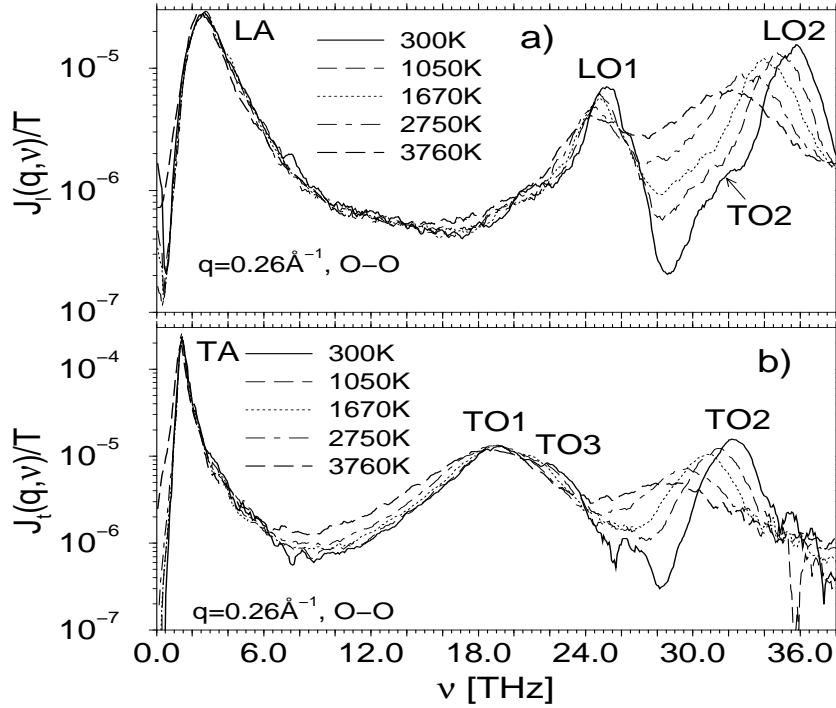


FIG. 6. Linewidth $\Gamma_{l,t}(q)$ obtained at $T = 2750$ K. The bold lines are power law fits with exponents 2 and 2.5 for $\Gamma_l(q)$ and $\Gamma_t(q)$, respectively. Also included are $\nu_l(q)$ (bold dashed line) and $\nu_t(q)$ (bold dotted line).



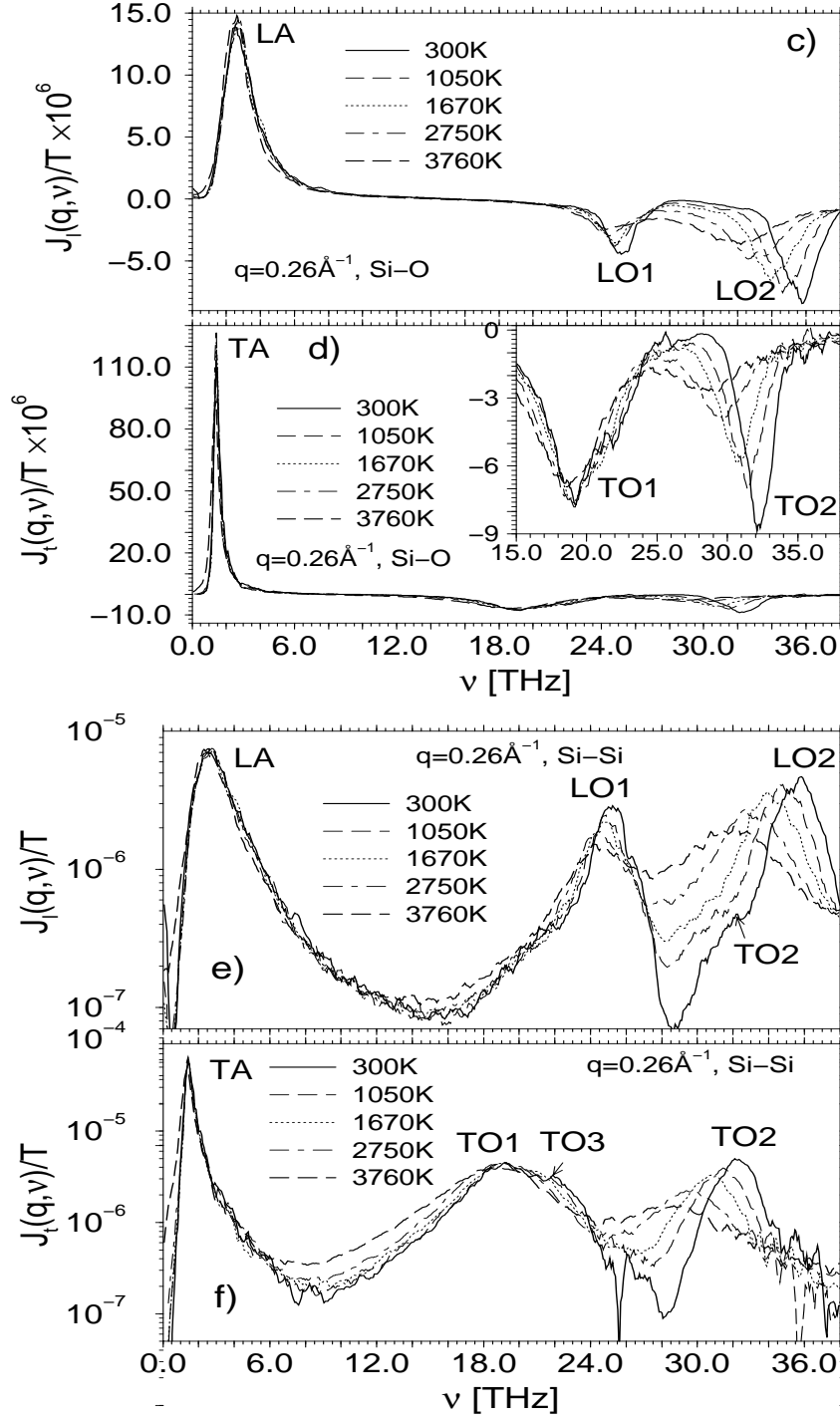


FIG. 7. The current correlation functions scaled with temperature for $q = 0.26 \text{ \AA}^{-1}$, a) $J_l(q, \nu)/T$ for the O-O correlations, b) $J_t(q, \nu)/T$ for the O-O correlations, c) $J_l(q, \nu)/T$ for the Si-O correlations, d) $J_t(q, \nu)/T$ for the Si-O correlations, e) $J_l(q, \nu)/T$ for the Si-Si correlations, f) $J_t(q, \nu)/T$ for the Si-Si correlations.

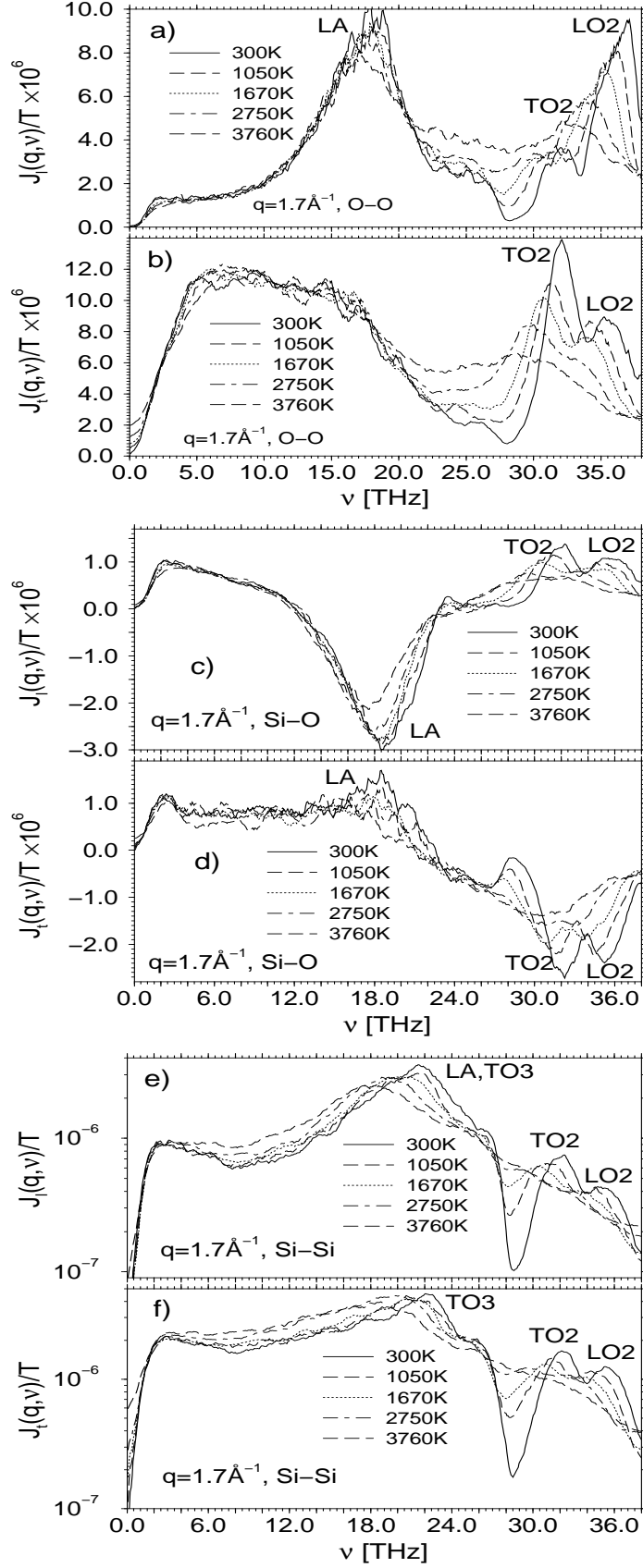


FIG. 8. The same as in Fig. 7 but now for $q = 1.7 \text{ \AA}^{-1}$.

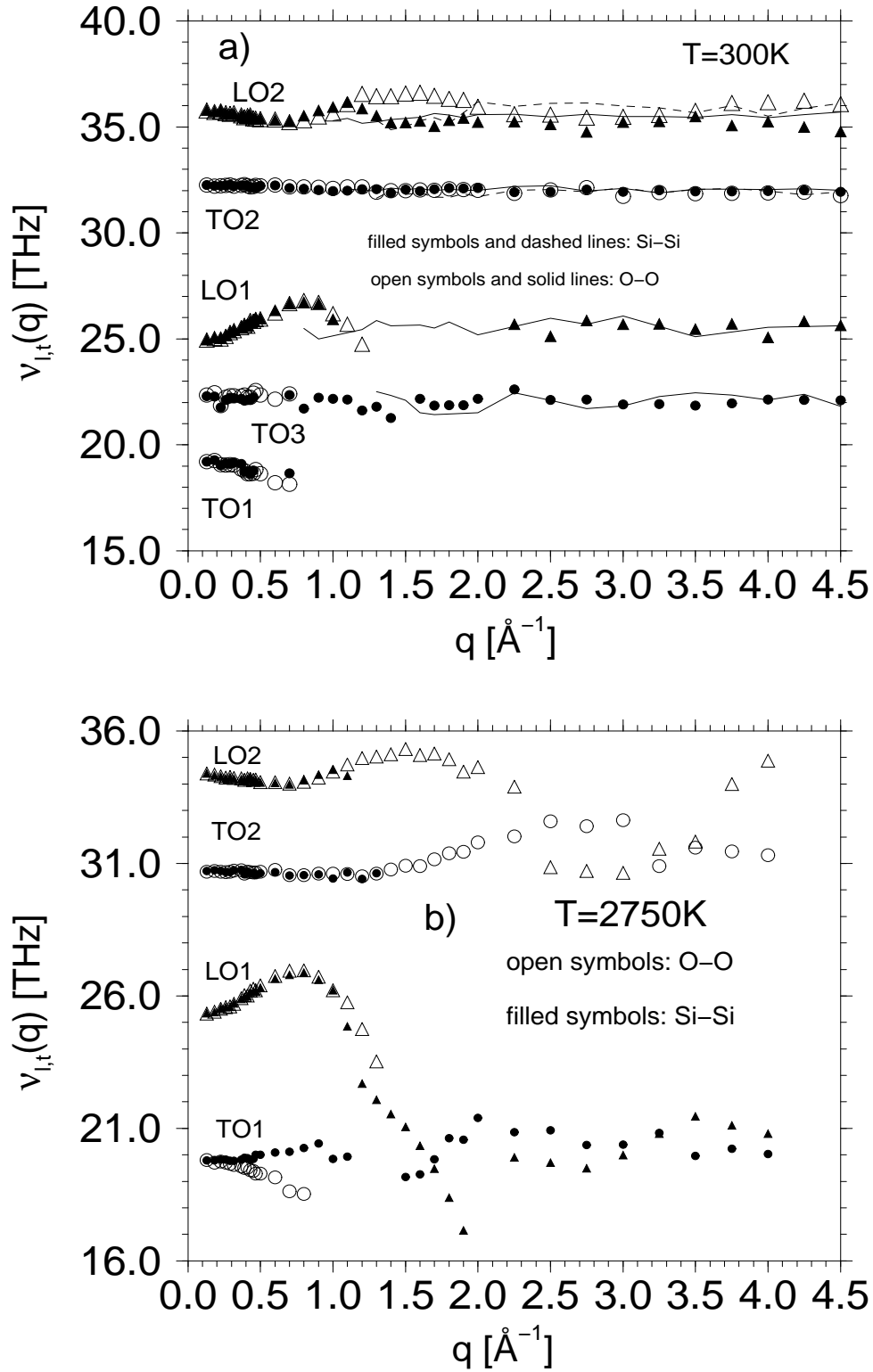
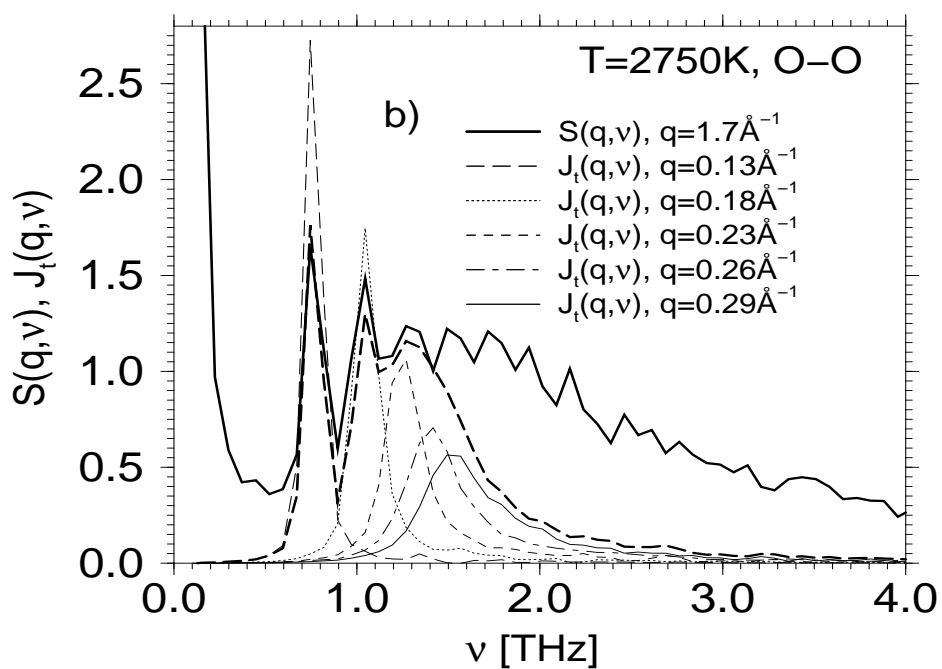
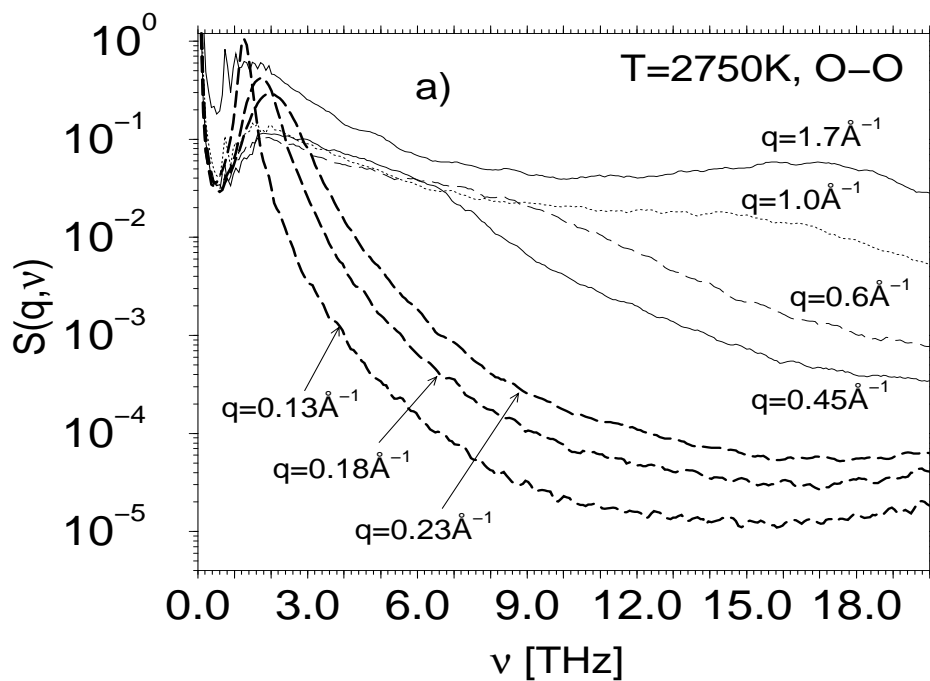


FIG. 9. Peak maximum position $\nu_{l,t}(q)$ of the excitations in the optical band for the Si-Si correlations (filled symbols) and the O-O correlations (open symbols) at a) $T = 300\text{ K}$ and b) $T = 2750\text{ K}$. See text for the explanation of the dashed and the solid line in a).



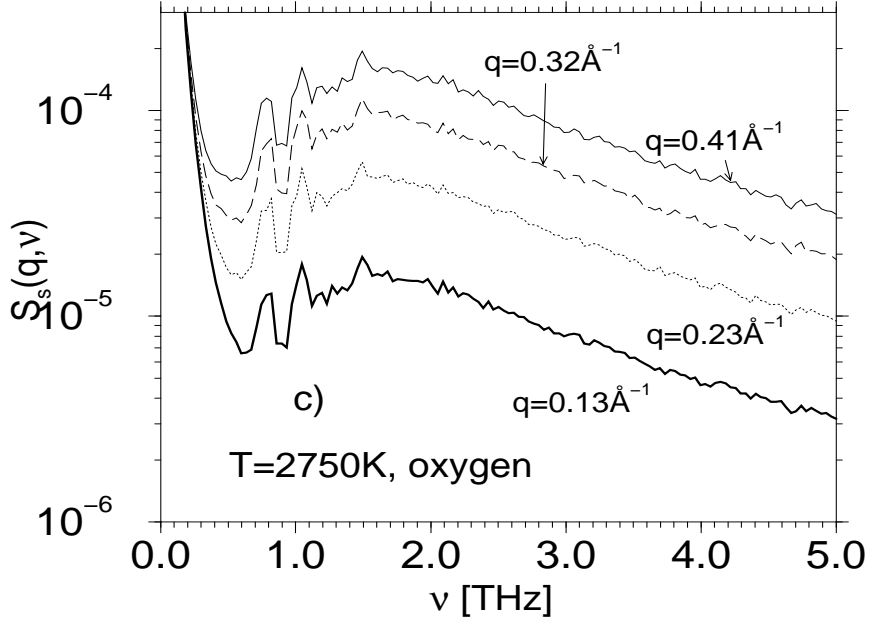


FIG. 10. a) Dynamic structure factor $S(q, \nu)$ for the O–O correlations at $T = 2750$ K for several values of q . b) $S(q, \nu)$ at $q = 1.7 \text{ \AA}^{-1}$ (bold solid line) and $J_t(q, \nu)$ for the five lowest q values of our simulation. The bold dashed line shows the sum of the latter current correlation functions divided by 1.6. c) Self part of the dynamic structure factor $S_s(q, \nu)$ for $q = 0.13 \text{ \AA}^{-1}$, $q = 0.23 \text{ \AA}^{-1}$, $q = 0.32 \text{ \AA}^{-1}$, and $q = 0.41 \text{ \AA}^{-1}$.

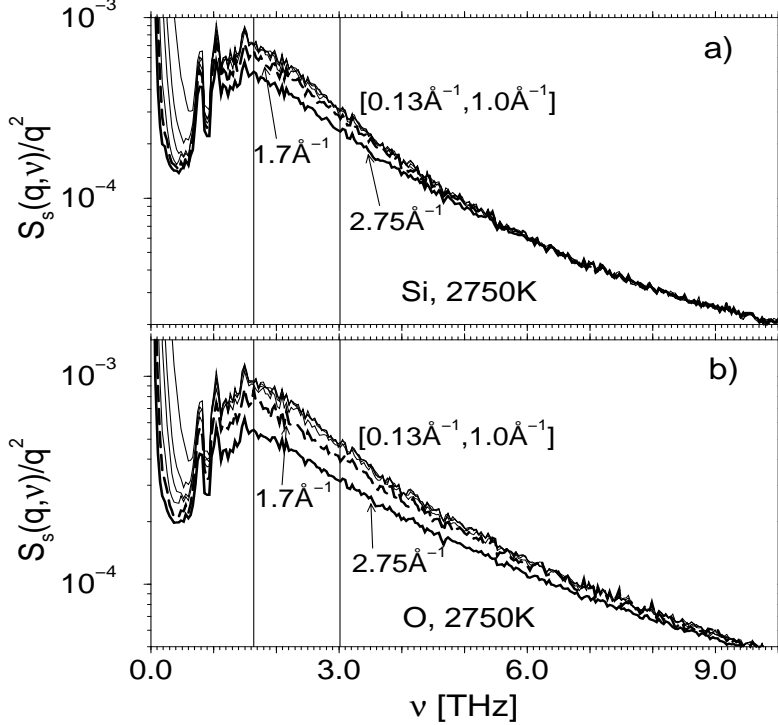


FIG. 11. Self part of the dynamic structure factor divided by q^2 for $q = 0.13 \text{ \AA}^{-1}$, 0.6 \AA^{-1} , 1.0 \AA^{-1} , 1.7 \AA^{-1} , and 2.75 \AA^{-1} for a) Si and b) O. The vertical lines are at the frequencies $\nu = 1.64$ THz and 3.02 THz at which the q dependence of $S(q, \nu)$ is shown in Fig. 12.

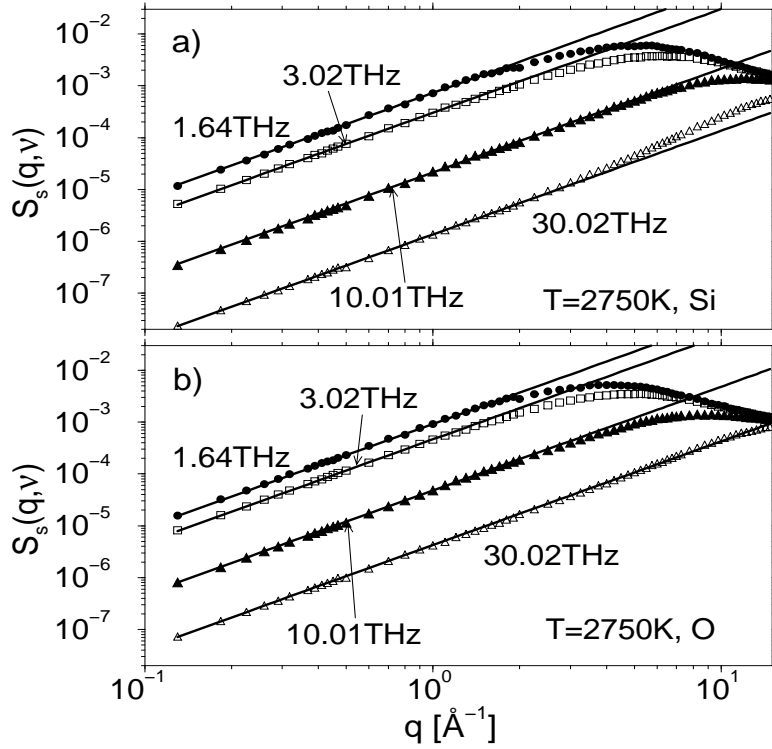


FIG. 12. q dependence of $S_s(q, \nu)$ for $\nu = 1.64$ THz, 3.02 THz, 10.01 THz, and 30.02 THz, for a) Si, and b) O. The bold straight lines are fits with q^2 laws.

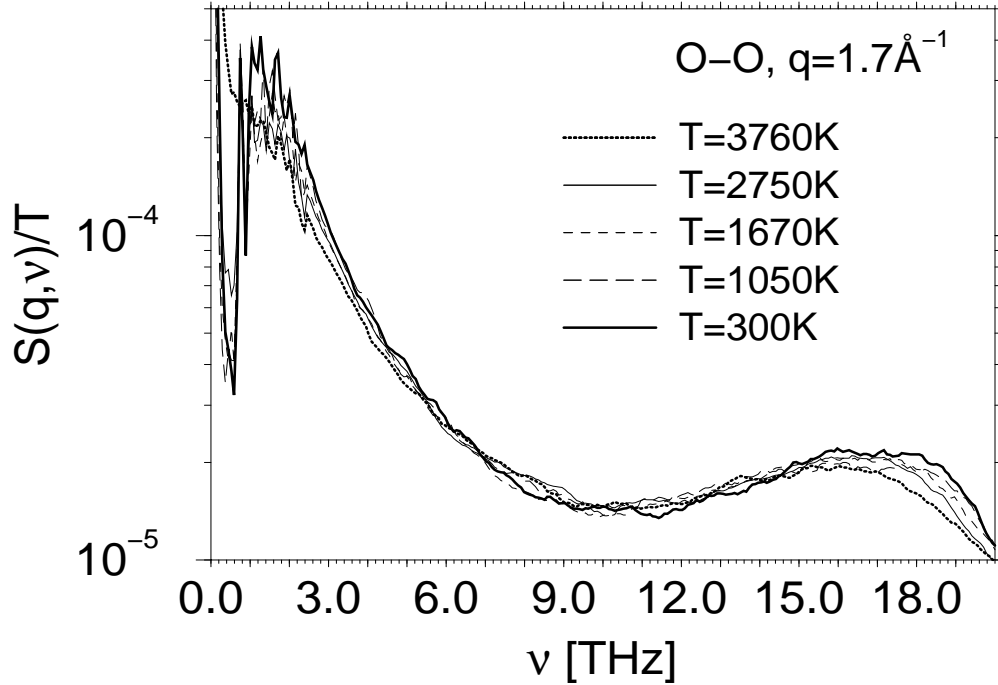


FIG. 13. $S(q, \nu)/T$ for the O-O correlations at $q = 1.7 \text{ \AA}^{-1}$ for the different temperatures.

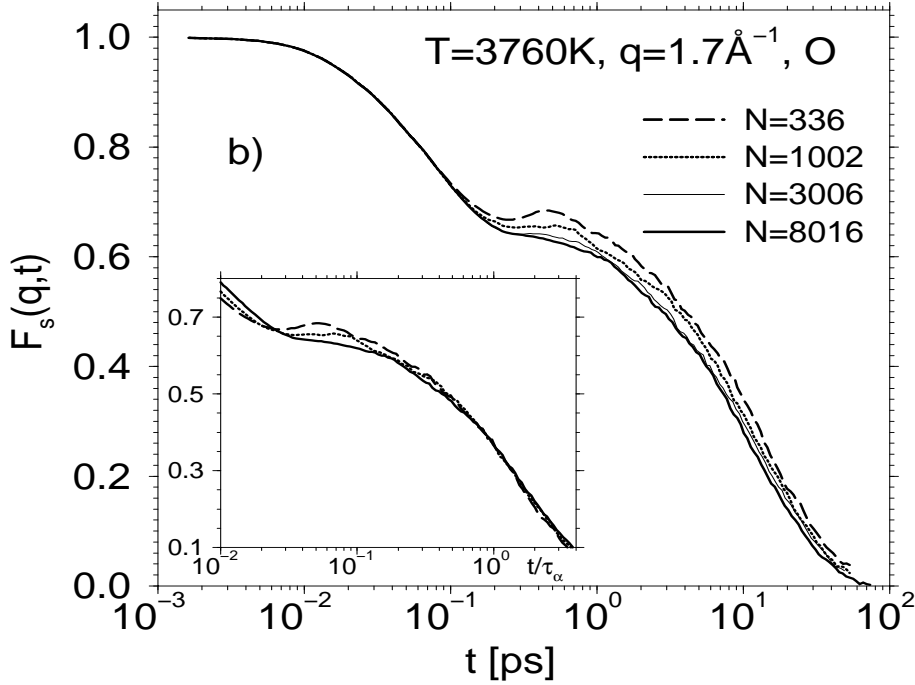
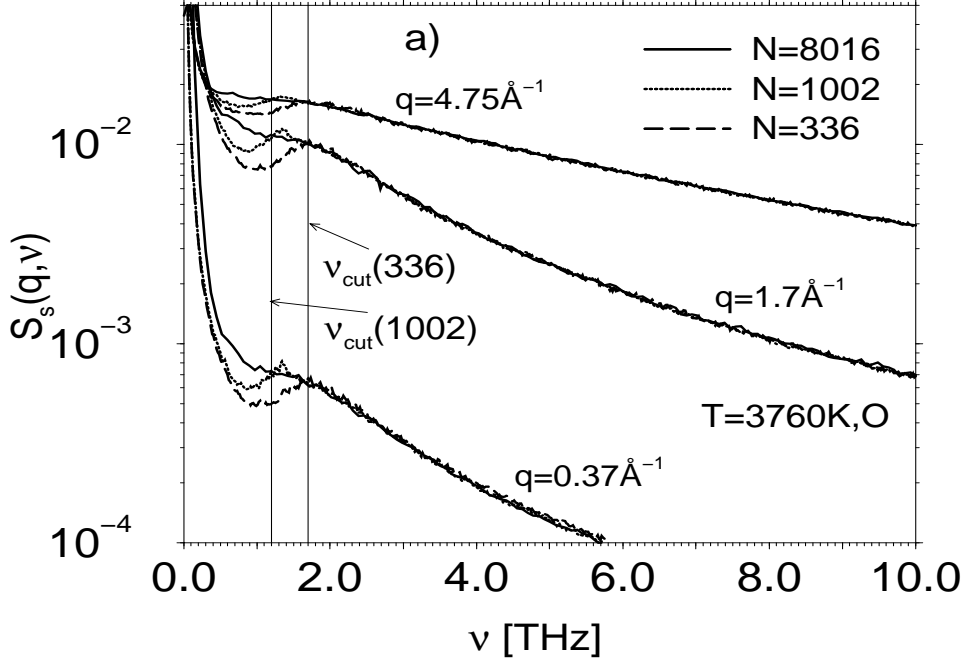
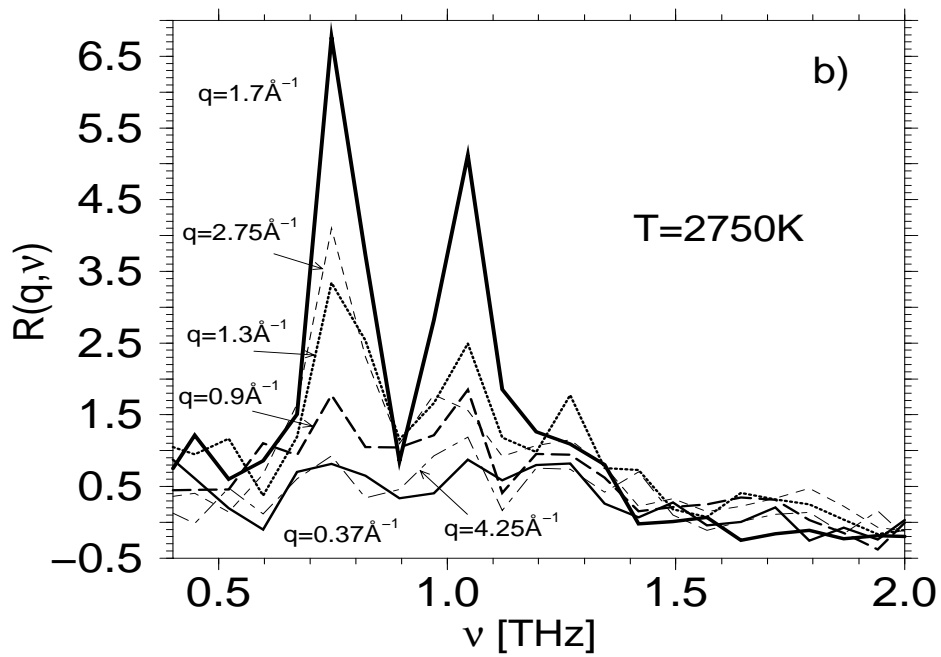
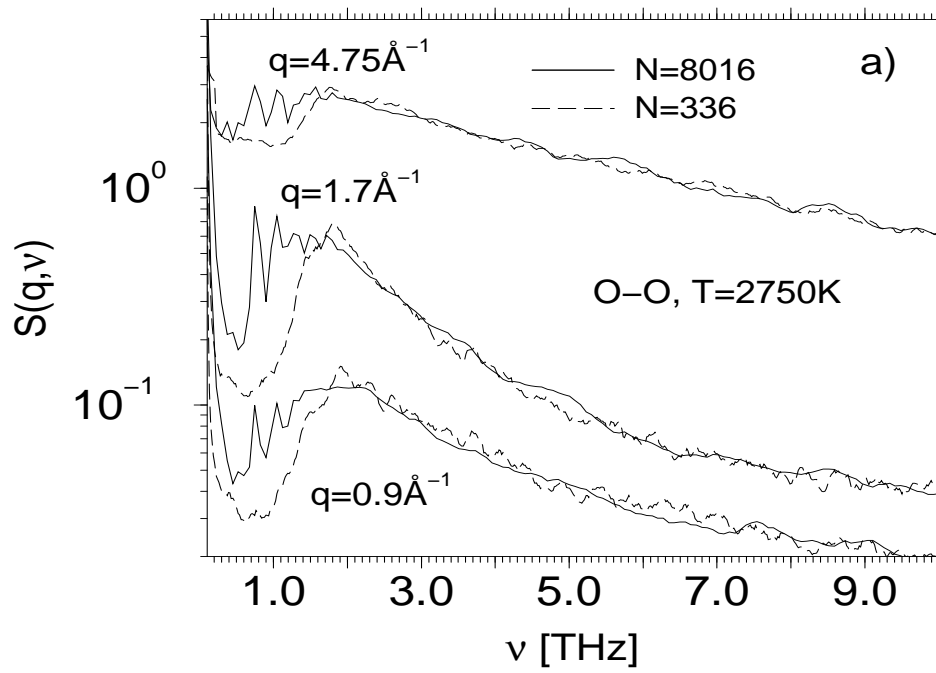


FIG. 14. a) The self part of the dynamic structure factor for oxygen for the different system sizes $N = 8016, 1002, 336$ at the wave-vectors $q = 0.37 \text{ \AA}^{-1}, 1.7 \text{ \AA}^{-1},$ and 4.75 \AA^{-1} , $T = 3760 \text{ K}$. See text for the explanation of the vertical lines. b) Incoherent intermediate scattering function for oxygen for the system sizes $N = 8016, 3006, 1002,$ and 336 at the wave-vector $q = 1.7 \text{ \AA}^{-1}$ and the temperature $T = 3760 \text{ K}$. The inset shows the same data (without the $N = 3006$ curve), plotted versus the scaled time t/τ_α .



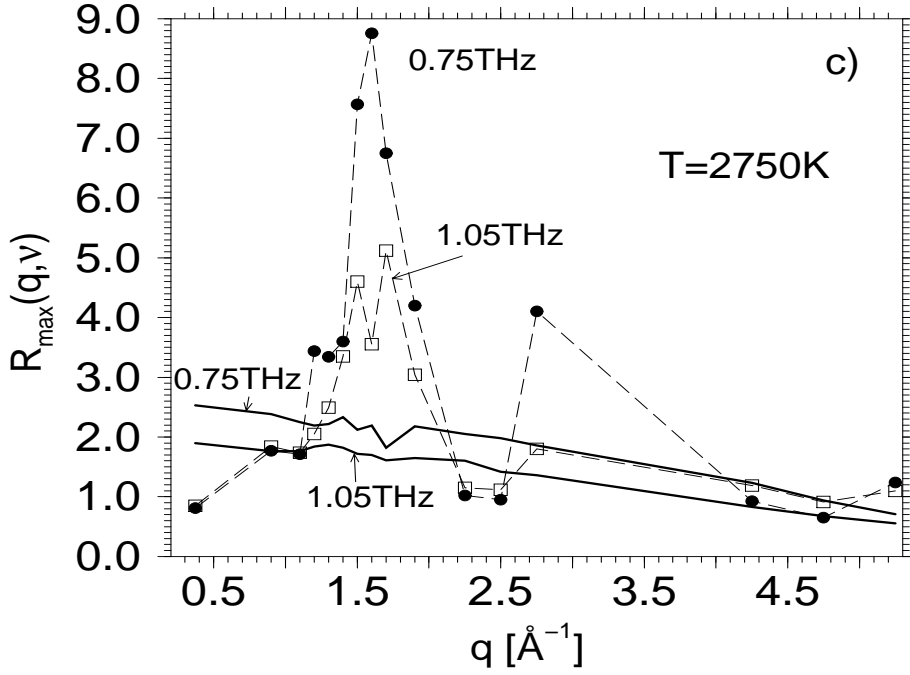


FIG. 15. a) The dynamic structure factor for the O-O correlations for the system sizes $N = 8016$ and $N = 336$ at the wave-vectors $q = 0.9 \text{ \AA}^{-1}$, 1.7 \AA^{-1} , and 4.75 \AA^{-1} and the temperature $T = 2750 \text{ K}$. b) $R(q, \nu)$ (definition see text) for several values of q as a function of frequency at $T = 2750 \text{ K}$. c) $R(q, \nu)$ for $\nu = 0.75 \text{ THz}$ (filled circles) and $\nu = 1.05 \text{ THz}$ (open squares) as a function of q at $T = 2750 \text{ K}$. Also included is $R_s(q, \nu)$ at the same frequencies obtained from $S_s(q, \nu)$ (bold lines).